ISSN 0915-6364

NATIONAL INSTITUTE FOR FUSION SCIENCE

Spectra of Neutral Carbon for Plasma Diagnostics

J.G. Wang, M. Kato and T. Kato

(Received - Sep. 14, 2000)

NIFS-DATA-58 Oct. 2000

RESEARCH REPORT
NIFS-DATE Series

TOKI, JAPAN

Spectra of Neutral Carbon for Plasma Diagnositics

J.G. Wang, M. Kato, and T. Kato
National Institute for Fusion Science
322-6 Oroshi-cho, Toki-shi 509-5292, Japan

October 2, 2000

Abstract

Recently, carbon pellet experiments have been perfomed on W-7AS and a few CI lines have been observed in the situation of the pellet cloud from the cold dense plasma to hot ambient plasma [1]. In so large varied conditions, the collisional radiative (CR) model is needed to study the spectra. In this article, a CR model including 79 states with $n \leq 6$ and $l \leq 4$ is developed, and then the line spectra and line intensity ratios are evaluated in the ionizing and recombining plasma, respectively.

keyword: carbon atom, dielectronic recombination, special lines, plasma dignostics, population density, ionization, recombination, excitation

1. Introduction

In the magnetic controlled fusion research, the impurity atoms and ions play an important role as a contributor for plasma cooling, due to its strong radiation with higher nuclear number. Meanwhile, the radiation also contains the information on the nature of plasma, and the spectroscopy of the radiation can be used to measure the plasma parameters. The radiation of plasma contains two parts: one is continuum spectra from the bremsstrahlung and radiative recombination, which often forms the background of line spectroscopy and can be used to measure the temperature of Maxwellian electron distrbution [2]; another is the line spectra from spontaneous radiation, which contain a lot of informations on the temperature and density of electron, and the ionization stages and excited state populations of partilly ionized ions. Using the intensity ratios and the profiles of some special lines, the electron temperature and density, and impurity temperature and density can be derived[3]. Carbon atom is one of the most important impurity species in the fusion edge plasma, since carbon composite materials are widely used as the first wall and divertor plate of fusion experimental devices. The line of 909.5 nm ($2p3p(^3P_2) \rightarrow 2p3s(^3P_2)$) has been widely used for the observation of CI line in takamaks like JET[4],TEXTOR[5], DITE[6] and a linear machine PISCES[7]. The lines of 155nm from CIV, 117.5nm and 97.7 nm from CIII and 133.4nm from CII have been observed in recent experiments[8], and the CII doublet ($^2P-^2S$) at 658nm and the CIII triplet ($^3P-^3S$) at 464.9nm have been used to measure the flow velocities of carbon ions in the DIII-D divertor[9].

In the practical diagnostic for plasma, we must provide spectral data with high accuracy, and then compare them to the experimental measurements. As is well known, the line spectra of plasma come from the spontaneous radiation of the excited atoms and the line intensities are proportional to the population of the excited states. In order to evaluate the population of excited states, several models have been proposed, that is, the corona and capture-cascade models for low electron-density regions and partial and complete LTE's for high-density regions. However, in the high density plasma corresponding to the edge or divertor plasma in the fusion devices, $n_e \sim 10^{11} - 10^{14} cm^{-3}$, the population density of the excited states must be determined by the collisional radiative (CR) model. Using CR model, the population dynamics in high density plasma as well as low density plasma has been investigated by Fujimoto[10] for hydrogen atoms in three different plasmas: equilibrium, ionizing and recombining plasma. So far, the population densities of hydrogen, helium and oxygen atoms/ions, which are investigated with the CR model, have been applied for the plasma parameter measurements[10, 11, 12]. As for atomic carbons, line emission profiles at 156.1 and 165.7nm from the solar chromosphere have been investigated[13, 14]. Sasaki et al.[15] have calculated the effective emission and ionization rate coefficients in the ionizing plasma with a CR model, in which 31 states including the ground state and the excited states with the principal quatumn number $n \leq 4$ and $l \leq 3$.

Recently, Sergeev et al.[1] have perfomed carbon pellet experiments on W-7AS, in which spherical carbon pellets of 0.3-0.5mm sizes and 200-300 m/sec velocities were injected in the direction of plasma core. They have observed a few CI lines. The situation of the pellet cloud plasma may change from the cold dense plasma (with cloud density $n_{CL} \sim 10^{15} - 10^{17} cm^{-3}$ and cloud temperature $T_{CL} \sim 1 - 50eV$) to hot ambient plasma (with electron density $n_e \sim (0.5 - 10)10^{13} cm^{-3}$ and temperature $T_e \sim 100 - 3000eV$). In so large varied condition, the CR model is needed to study the spectra in both ionizing and recombining plasma. In this article, using the CR model including 79 states with the principal quatumn number $n \leq 6$ and $l \leq 4$, we calculate the line spectra and line intensity ratios in the ionizing and recombining plasma, and dicussed the theoretical method in equilibrium and non-equilibrium plasma.

2. RATE EQUATION

We consider the rate equation for neutral carbon, in which the carbon atom CI and carbon ion CII are involved, and these carbon ions with more than one charge are not included. The population densities of the i-th state of carbon atoms, n(i), is described by the following rate equation:

$$\begin{aligned} \frac{dn(i)}{dt} &= \{\sum_{j \neq i} n_e C_{ji} n(j) + \sum_{j>i} A_{ji} n(j)\} \\ &\quad -\{\sum_{j \neq i} n_e C_{ij} n(i) + \sum_{j<i} A_{ij} n(i)\} \\ &\quad -\sum_k n_e S_{ik} n(i) + \sum_k n_e \alpha_{ki} n_+(k), \end{aligned} \tag{1}$$

where n_e is the electron density and $n_+(k)$ is the population density in the k-th state of a singly charged ion. The collisional excitation, de-excitation and ionization by electron impact are taken into account in our calculation. The collisional processes with ion and atom impact are neglected. C_{ji} is the electron impact excitation rate coefficient and A_{ji} is the radiative transition probability from j-th to i-th state. S_{ik} is the electron impact ionization rate coefficient for which a neutral atom in the i-th state is ionized into the k-th stae of singly ionized charged ion. α_{ki} is the recombination rate coefficient where a singly charged ion in the k-th state recombines into the i-th state of a neutral atom. The radiative recombination, dielectronic recombination and three-body recombination (the inverse electron impact ionization) are included as recombination processes in our cacu-lation. We consider 79 states as summarized in Fig.1, in which the splitting of terms for $2p5g$ and $2p6g$ are not included.

According to the method of the quasi-steady-state solution[10], for all the excited states, eq. (1) is assumed to be 0, that is, $dn(i)/dt = 0$ for $i = m, m+1..., 79$, $m-1$ is the number of ground state and metastable states. Futhermore, it is supposed that a minority of impurity carbon is immersed in the plasma and the change of its ionizing degree doesn't cause the increase or decrease in the electron density, then we have a set of the coupled linear equations, which contain $n(p)(p = 1, ..., m)$ and $n_+(k)$ as parameters. Based on the linear algebraic theory, the population of excited states can be solved in the form

$$n(i) = \sum_k r_0(i,k) n_+(k) + \sum_p r_1(i,p) n(p), \qquad (2)$$

where $r_0(i,k)$ is the contribution of the singly ionized ion to the excited state i, and $r_1(i,p)$ is the contribution of the ground state in neutral atom to the excited state. For recombination processes from the singly ionized ion, the summation on k only has one term in eq. (2), and if we treat the metastable states as other excited states to be quasi steady states, the summation on p also have one term. In our calculation we take into account only the ground state for both $n_+(k)$ and $n(p)$ in eq.(2) as

$$n(i) = r_0(i) n_+ + r_1(i) n(1), \qquad (3)$$

which means that the population of excited states is the sum of two components. If we treat the first and second terms in eq. (3) separately, the first term is called the recombining plasma componet, whereas the second term is called the ionizing plasma component.

The rate equation, eq. (1), for the ground state is rewritten in terms of $r_0(i)$ and $r_1(i)$ for $i \geq 2$, viz.

$$\frac{dn(1)}{dt} = -S_{CR} n(1) n_e + \alpha_{CR} n_+ n_e, \qquad (4)$$

where S_{CR} and α_{CR} are the collisional-radiative ionization and recombination rate coefficients, respectively, are functions of n_e and T_e:

$$S_{CR} = \sum_{j>1} C_{1j} - \sum_{j>1} [C_{j1} + A_{j1}/n_e] r_1(j) + S_{11} \qquad (5)$$

and

$$\alpha_{CR} = \sum_{j>1} [C_{j1} + A_{j1}/n_e] r_0(j) + \alpha_{11} \qquad (6)$$

When $dn(1)/dt = 0$ or $S_{CR} n(1) n_e = \alpha_{CR} n_+ n_e$, the plasma is called the ionization equilibrium plasma.

3. Atomic Data

Collisional excitations from the ground states ($2p^2(^3P)$) and from the two metastable states ($2p^2(^1D)$ and $2p^2(^1S)$) to the other excited states and from the excitation states to the excitation states for the allowed transitions are taken into accout. We also include the forbidden transitions whose initial and final states have the same configuration but different terms. Some of the rate coefficients for $n \leq 4$ are calculated by R-matrix[16], and the others are calculated on Mewe's semi-empirical formula[17] using the oscillator strength f_{ij} and excitation energy E_{ij}[18, 19, 20, 21]. Electron impact ionization from all the excited states are included, and the rate coefficients are estimated by Lotz's empirical formula[22]. The collisional de-excitation and three-body recombination rate coefficients are derived by detailed balance from the excitation and ionization rate coefficients. The spontaneous radiative processes for all the allowed transitions and three forbidden transitions, $2p^2(^1D)-2p^2(^3P)$, $2p^2(^1S)-2p^2(^3P)$, $2p^2(^1S)-2p^2(^1D)$, are included[18, 19, 20, 21, 23]. Radiative recombination rate coefficients are obtained by detailed balance from the photoionization cross sections[24].

Dielectronic recombination rate coefficients to each excited state are calculated by Cowan's code[25, 26] for $n \leq 6$ and are used in our calculation. The collisional density effect of plasma on rate coefficients in

high n states have been derived from the n- distribution of the dielectronic rate coefficients[25, 26]. This effect have been included by multiplying a modified factor F which is calculated by the following formula,

$$F = \begin{cases} 0.128ln(n_t) - 0.213 & \text{if } 4 < n_t \leq 20 \\ 0.296ln(n_t) - 0.758 & \text{if } 20 < n_t \leq 100 \\ 1.13exp(-63.8/n_t) & \text{if } 100 < n_t \end{cases} \quad (7)$$

where n_t is the thermal limit of Rydberg states, which can be evaluated by Griem's formula,

4. Result and Discussion

In our calculation, the contribution to the excited states is divided into two components, that is, the ionizing and recombining components. For the realistic plasma, it should be a summation of the two components. In order to sum the two components, we need to obtain the relative population of $n(1)$ and n_+. When the time scale of plasma parameters is much larger than that of ionization ($\sim 1/(n_e \cdot S_{CR})$) and recombination ($\sim 1/(n_e \cdot \alpha_{CR})$), the plasma is in the ionization equilibrium or near-equilibrium, and then we can use the equilibrium value $n(1)/n_+ = \alpha_{CR}/S_{CR}$ to calculate the spectra. Of course, there exist some case, in which one process (ionization or recombination) dominants over another (recombination or ionization)[10] and we only need to consider one process (ionization or recombination), it depends on the plasma temperature, density and the relative population of $n(1)$ and n_+. In the large varied condition on carbon pellet experiments[1], both the ionizing and recombining components should be considered. In Fig.2, we plotted the collisional-radiative ionization and recombination rate coefficients. It can be found, when $T_e >$ 2 eV, the collisional-radiative ionization rate coefficients are much larger than the collisional-radiative recombination rate coefficients, in the equilibrium or near-equilibrium region, $n(i) \gg n_+$, the ionizing process dominates the recombining process; when $T_e <$ 0.8 eV, the collisional-radiative recombination rate coefficients are much larger than the collisional-radiative ionization rate coefficients, in the equilibrium or near-equilibrium region, $n(i) \gg n_+$, the recombining process dominate over the ionizing process; when $0.8eV < T_e < 2eV$, both the ionizing and recombining components contribute to the population densities. In Fig.3, we plot the population density of ionizing ($r_1(i)/n_e$) and recombining component ($r_0(i)/n_e$) for the excited states $2p3l$. The population for $2p4l$, $2p5l$ and $2p6l$ are similar to $2p3l$.

In previous papers[15], the population dynamics has been discussed in detailed. In this paper, we will concentrate on the spectra and line intensity ratios for plasma diagnostic in the ionizing and recombining plasma.

4.1 Ionizing Plasma

We assume that there is one neutral carbon atom in the ground state, and then the line intensity from j to i is expressed as,

$$I_{ji} = n(j)A_{ji} \quad (8)$$

here the unit of I_{ji} is $photons \cdot s^{-1} \cdot atom^{-1}$. The spectra are synthesized with Gaussian distribution with the assumed full width of half maximum (FWHM) $\Gamma = 0.1nm$,

$$J_{ji}(\lambda) = \frac{I_{ji}}{(2\pi)^{1/2}\Gamma} exp\Big[-\frac{(\lambda - \lambda_{ji})^2}{2\Gamma^2}\Big] \quad (9)$$

here λ_{ji} is the photon wavelength from j to i. The units of λ, λ_{ji} and $J_{ji}(\lambda)$ are nm, nm and $photons \cdot s^{-1} \cdot nm^{-1} \cdot atom^{-1}$.

4.1.1 Spectra

The spectra of neutral carbon at $T_e = 10eV$ and $n_e = 10^{10}cm^{-3}$ in the ionizing plasma are shown in Fig.4. We plot the total spectra in the wavelength from 100 to 1000 nm , and detailed spectra in the wavelength from 100 to 200 nm, 550 to 650 nm and 900 to 1000 nm, as shown in Fig.4 (a), Fig.4 (b), Fig.4 (c), Fig.4 (d), respectively. The spectra can be divided into four regions approximately: From 100 to 200 nm, the contributions to the spectra come from the transition $2pnl(n \geq 3)$ to $2p^2$ with different terms; from 480 to 540 nm, the contributions come from the transition $2pnp(n \geq 4)$ to $2p3s$; from 550 to 740 nm, the contributions come from the transition $2pnd(n \geq 4)$ to $2p3p$ with different terms, especially, the largest contributions come from the transition $n = 4$, because the states with the lower principal quantum number have the larger populations; from 800 to 1000 nm, the contributions come from the transition $2p3p$ to $2p3s$.

In Fig.5, we plot the spectra at $T_e = 100eV$ and $n_e = 10^{10}cm^{-3}$. Compared to Fig.4, the intensities from the states with the higher $n(n \geq 4)$ increase

much more than the states with the lower $n(n \leq 4)$, because there are more neutral atoms excited to the high excited states from the ground states with the increasing temperature. In Fig.6 and Fig.7, we plot the spectra of neutral carbon at the same electron density $n_e = 10^{14} cm^{-3}$ and different electron temperature $T_e = 10eV$, $T_e = 100eV$, respectively. Compared to Fig.4 and Fig.5, the intensities are two magnitude higher than that in Fig.4 and Fig.5.

4.1.2 Line intensity ratio

The line intensity ratio can be calculated by

$$\frac{I_{ji}}{I_{j'i'}} = \frac{n(j)A_{ji}}{n(j')A_{j'i'}}. \qquad (10)$$

In Fig.8 (a), Fig.8 (b) and Fig.9 (a), we plot the line intensity ratios among 3 lines denoted in Fig.2 (d): 912 nm ($2p3p(^3P) \rightarrow 2p3s(^3P)$) (triplet line), 939 nm ($2p3p(^1D) \rightarrow 2p3s(^1P)$) (singlet line), and 968 nm ($2p3p(^3S) \rightarrow 2p3s(^3P)$) (triplet line). The line intensity ratio between triplet lines varies slowly with the temperature and density, as shown in Fig.8 (a); however, the line intensity ratio between triplet and singlet lines varies rapidly with the temperature and density, as shown in Fig.8 (b) and Fig.9 (a), it is because the triplet lines come from the ground states (triplet state) by collisional excitation and the singlet lines comes from the mestable states (singlet state). So for the plasma diagnostics, it is better to use the line intensity ratios between triplet and singlet lines.

In Fig.9 (b), Fig.10 (a) and Fig.10 (b), we plot the line intensity ratios among some lines denoted in Fig.4 (c): 602 nm ($2p5d(^3F) \rightarrow 2p3p(^3D)$) /605 nm ($2p6s(^3P) \rightarrow 2p3p(^3D)$); 579 nm ($2p5d(^1D) \rightarrow 2p3p(^1P)$) /635 nm ($2p5d(^3P) \rightarrow 2p3p(^3S)$); 585 nm ($2p6d(^3P) \rightarrow 2p3p(^3S)$) /579 nm ($2p5d(^1D) \rightarrow 2p3p(^1P)$).

In fact, for the realistic plasma diagnotics, we must consider the line intensity enough to be measured, the experimental resolution enough to distingush the different lines and the variation of line intensity ratios with the electron temperature and density. In Fig.11 (a), Fig.11 (b), Fig.12 (a) and Fig.12 (b), we plot the line intensity ratios among some lines denoted in Fig.4 (b): 156 nm ($2p5d(^1P) \rightarrow 2p^2(^1S)$) /160 nm ($2p4d(^1P) \rightarrow 2p^2(^1S)$); 160 nm ($2p4d(^1P) \rightarrow 2p^2(^1S)$) /175 nm ($2p3d(^1P) \rightarrow 2p^2(^1S)$); 126 nm ($2p3d(^3P) \rightarrow 2p^2(^3P)$) /193 nm ($2p3s(^1P) \rightarrow 2p^2(^1D)$); 160 nm ($2p4d(^1P) \rightarrow 2p^2(^1S)$) /126 nm ($2p3d(^3P) \rightarrow 2p^2(^3P)$).

It can be seen that the line intensity ratios involving the same Rydberg series, such as $2p5d(^1P)$ and $2p4d(^1P)$ in Fig.11 (a), $2p4d(^1P)$ and $2p3d(^1P)$, is not suitable for plasma diagnostic, because they have the similar behavior on the electron temperature and density, and their line intensity ratios varies slowly with the electron temperature and density, although they are easy to be distingushed in the experiments.

4.2 Recombining Plasma

There are three kinds of recombination processes in plasma, that is, the radiative recombination, dielectronic recombination and three-body recombination. At low electron density and low temperature ($T_e < 1eV$), the main contribution to recombination comes from the radiative recombination process, and at low electron density and high temperature ($T_e > 1eV$), the main contribution comes from the dielectronic recombination process. At high electron density, the main contribution come from the three-body recombination process, especially, at low electron temperature. In the calculation of the spectra in recombining plasma, the continuum spectra for the radiative recombination have also been included, which can be written as,

$$\begin{aligned} J_c(\lambda) &= 2(\frac{2\kappa T}{\pi m_e})^{1/2} exp(-\frac{E_{h\nu} - E_I}{\kappa T}) \cdot \\ &\quad \frac{E_{h\nu} - E_I}{\kappa T} \cdot \frac{E_{h\nu}}{\kappa T} \cdot \frac{E_{h\nu}}{hc} \cdot \sigma_r \cdot n_e, \\ &\quad \text{when } E_{h\nu} > E_I \end{aligned} \qquad (11)$$

here κ is Boltzmann constant, $E_{h\nu}$ is the energy of photon produced by radiative recombination, E_I is the photo-ionization threshold, σ_r is the cross section of radiative recombination. We also included the satellite spectra in dielectronic recombination processes using the numerical data[25].

4.2.1 Spectra

The spectra of neutral carbon at $T_e = 0.5eV$ and $n_e = 10^{10} cm^{-3}$ in the recombining plasma are shown in Fig.13. We plot the total spectra in the wavelength from 100 to 1000 nm, and detailed spectra in the wavelength from 100 to 200 nm, 550 to 650 nm and 900 to 1000 nm, as shown in Fig.13 (a), Fig.13 (b), Fig.13 (c), Fig.13 (d), respectively. The continuum spectra in Fig.13(b) come from the radiative recombination to the ground state and mestable states, and the continuum spectra in Fig.13(c) come from the

radiative recombination to the excited states. The satellite spectra in dielectronic recombination processes is too weak to be seen. In Fig.14, we plot the spectra at $T_e = 1.0eV$ and $n_e = 10^{10}cm^{-3}$. Compared to Fig.13, for the line spectra, there is no large difference, this is because the rate coefficients between 0.5eV and 1.0eV are the same values; but the continnum spectra become wide due to the increase of temperature as seen in eq.(11). The small peak at about 820 nm is the contribution of satellite lines, but in general, its contribution can be ignored. In Fig.15 and Fig.16, we plot the spectra of neutral carbon at the same electron density $n_e = 10^{14}cm^{-3}$ and different electron temperature $T_e = 0.5eV$, $T_e = 1.0eV$, respectively. Compared to Fig.13 and Fig.14, the intensities are six magnitude higher than that in Fig.13 and Fig.14, and the relative importance of the contuinuum spectra is decreased, because the main recombination contribution come from three-body recombination processes and not the radiative recombination.

4.2.2 Line intensity ratio

In Fig.17 (a) and Fig.17 (b), we plot the line intensity ratios:
912 nm ($2p3p(^3P) \rightarrow 2p3s(^3P)$) /968 nm ($2p3p(^3S) \rightarrow 2p3s(^3P)$) and 912 nm ($2p3p(^3P) \rightarrow 2p3s(^3P)$) /939 nm ($2p3p(^1D) \rightarrow 2p3s(^1P)$).

At high electron density in the recombining plasma, the main contribution come from the three-body recombination processes, the line intensity ratios varies slowly with the temperature and density and can not be used for the palsma diagnostics. Only when the electron density is not very high, and the dielectronic recombination process gives an important contribution, the line intensity ratio can be used. Because dielectronic recombination is a resonant process, its rate coefficients have the different temperature-dependent behavior, as shown in Fig.18 and Fig.19 for $2p3s(^3P)$ and $2p3p(^3S)$.

In Fig.20, Fig.21, Fig.22 and Fig.23, we plot the line intensity ratios, respectively:
968 nm ($2p3p(^3S) \rightarrow 2p3s(^3P)$) /939 nm ($2p3p(^1D) \rightarrow 2p3s(^1P)$), 602 nm ($2p5d(^3F) \rightarrow 2p3p(^3D)$) /605 nm ($2p6s(^3P) \rightarrow 2p3p(^3D)$); 579 nm ($2p5d(^1D) \rightarrow 2p3p(^1P)$) /635 nm ($2p5d(^3P) \rightarrow 2p3p(^3S)$), 585 nm ($2p6d(^3P) \rightarrow 2p3p(^3S)$) /579 nm ($2p5d(^1D) \rightarrow 2p3p(^1P)$); 156 nm ($2p5d(^1P) \rightarrow 2p^2(^1S)$) /160 nm ($2p4d(^1P) \rightarrow 2p^2(^1S)$), 160 nm ($2p4d(^1P) \rightarrow 2p^2(^1S)$) /175 nm ($2p3d(^1P) \rightarrow 2p^2(^1S)$); 126 nm ($2p3d(^3P) \rightarrow 2p^2(^3P)$) /193 nm ($2p3s(^1P) \rightarrow 2p^2(^1D)$), 160 nm ($2p4d(^1P) \rightarrow 2p^2(^1S)$) /126 nm ($2p3d(^3P) \rightarrow 2p^2(^3P)$).

For the plasma that the ionization and recombination components are mixed, after the relative populations of n(1) and n_+ are obtained, the spectra can be calculated by simple summation. However for the line intensity ratios, we must calculate the population of the excited states from the two components firstly, and then calculate the line intensity ratios using the eq.(10).

We have studied the emission of carbon atom in plasma with the use of collisional radiative model including both ionizing component and recombibning component. We have presented the effective ionization and recombination rate coefficients as a function of electron density and temperature as well as the spectra and line intensity ratios.

This work was partily supported by the Japan Sociaty for Promotion of Science.

References

[1] V. Sergeev, L. Ledl and R. Burhenn, private communication, 1998.

[2] J.E. Rice, K. Molvig, and H.I. Helava, Phys. Rev. **A 25** (1982)1645.

[3] D. Salzmann, Atomic Physics in Hot Plasma (Oxford University Press, 1998).

[4] P. C. Stangeby, J. Nucl.Mater. **176** & **177** (1990) 51.

[5] E. Hintz and P. Bogen, J. Nucl.Mater. **128** & **129** (1984) 229.

[6] D.H. Goodall, S.J. Fielding, C.S. Pitcher, J. Allen and D.M. McCracken, J. Nucl. Mater. **145-147** (1987)596.

[7] Y. Ra, A. Pospieszczyk, Y. Hirooka, W.K. Leung and R. W. Conn, J. Vac. Sci. Technol. **A8** (1990)1783.

[8] M.E. Fenstermacher, J. Boedo, R.C. Isler et al., Plasma Phys. Control. Fusion **41** (1999)A345.

[9] R.C. Isler, N.H. Brooks, W.P. West, G.D. Porter and DIII-D Divertor Team, Phys. Plasmas **6** (1999)1837.

[10] T. Fujimoto, J. Phys. Soc. Jpn. **47** (1979)265, **47** (1979)272, **49** (1980)1561, **49** (1980)1569, **54** (1985)2905; J. Quant. Spectrosc. Radiat. Transfer **21** (1979)439.

[11] T. Kato, K. Masai and J. Mizuno, J. Phys. Soc. Jpn. **52** (1983)3019.

[12] K. Masai, Research Report NIFS-209 (National Institute for Fusion Science, Nagoya, 1993)

[13] R.A. Shine, B.W. Lites and E.G. Chipman, Astrophys. J. **224**(1978)247.

[14] P. J. Mauas, E.H. Avrett and R. Loeser, Astrophys. J. **345** (1989) 1104.

[15] S. Sasaki, Y. Ohkouchi, T. Takamura and T. Kato, J. Phys. Soc. Jpn. **63** (1994) 2942.

[16] K.M. Dunseath, V.M. Burke, P.G. Burke, A.E. Kingston, R.H.G. Reid and J.H. Tait, JET Order No:JP2/11566(1993); W.C. Fon, V.M. Burke, P.G. Burke, K.M. Dunseath, A.E. Kingston, R.H.G. Reid and J.H. Tait, JET Order No:JP2/11566(1994)

[17] R. Mewe, Astron. Astrophys. 20(1972)215.

[18] G.A. Victor and V. Escalante, Atomic Data and Nuclear Data Tables **40** (1988)203.

[19] B.C. Fawcett, Atomic Data and Nuclear Data Tables **37** (1987)411.

[20] D. Luo and A.K. Pradhan, J. Phys. **B: 22** (1989)3377.

[21] W. Wiese, National Standard Reference Data Series **4** (National Bureau of Standard, 1966) Vol. 1.

[22] W. Lotz, Z. Physik **216** (1968)1679.

[23] U. Safronova, private communication (1998).

[24] R.E.H. Clark, R.D. Cowan, and F.W. Bobrowicz, Atomic Data and Nuclear Data Tables **34** (1986)415.

[25] U. Safronova and T. Kato, J. Phys. **B 31** (1998)2501.

[26] T. Kato, U. Safronova and J. Dubau, NIST Special Publication **926**, ICAMDATA 97, edited by W. Wiese and P.J. Mohr, p.30 (1997).

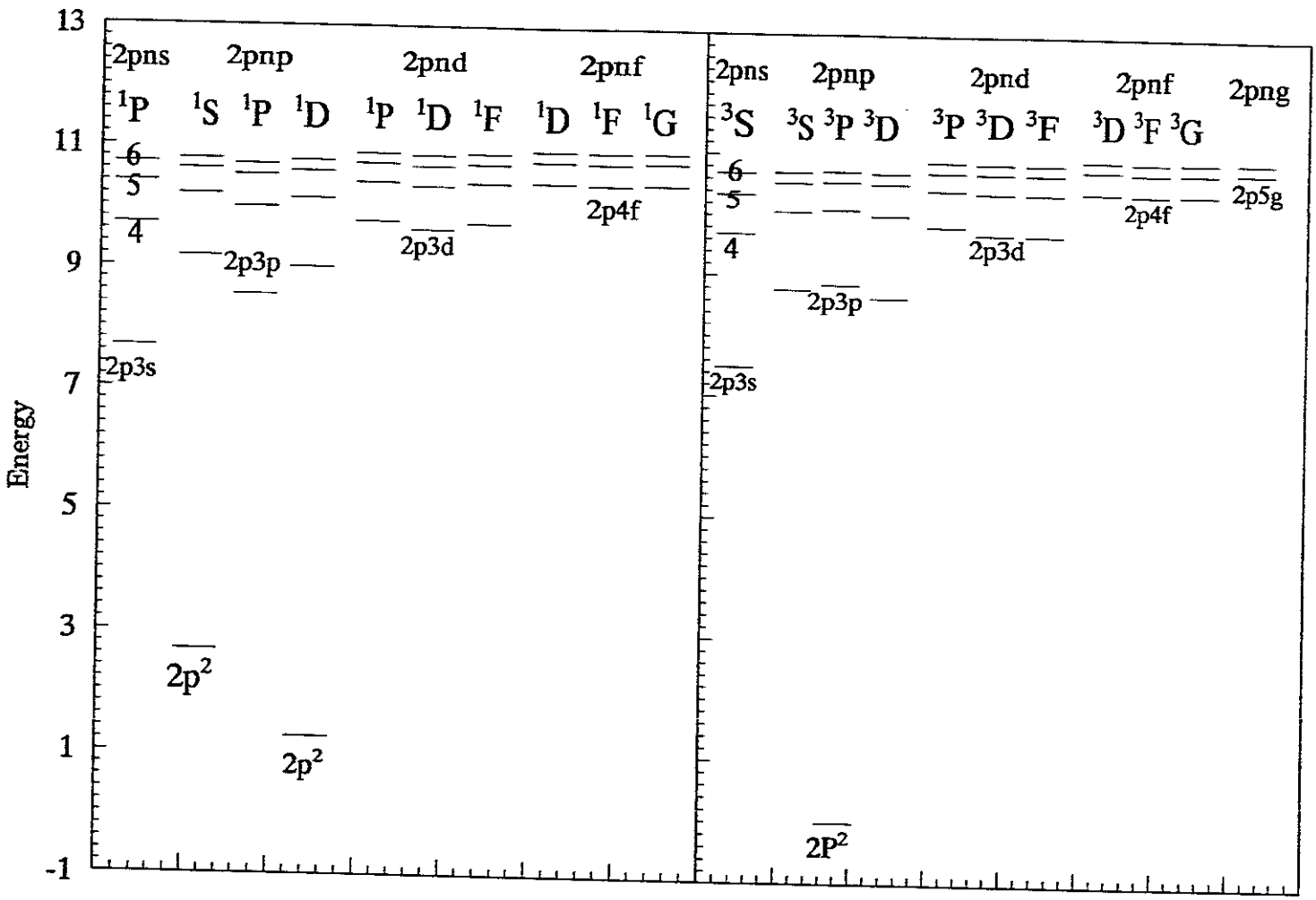

Fig.1 The included energy levels for neutral carbon

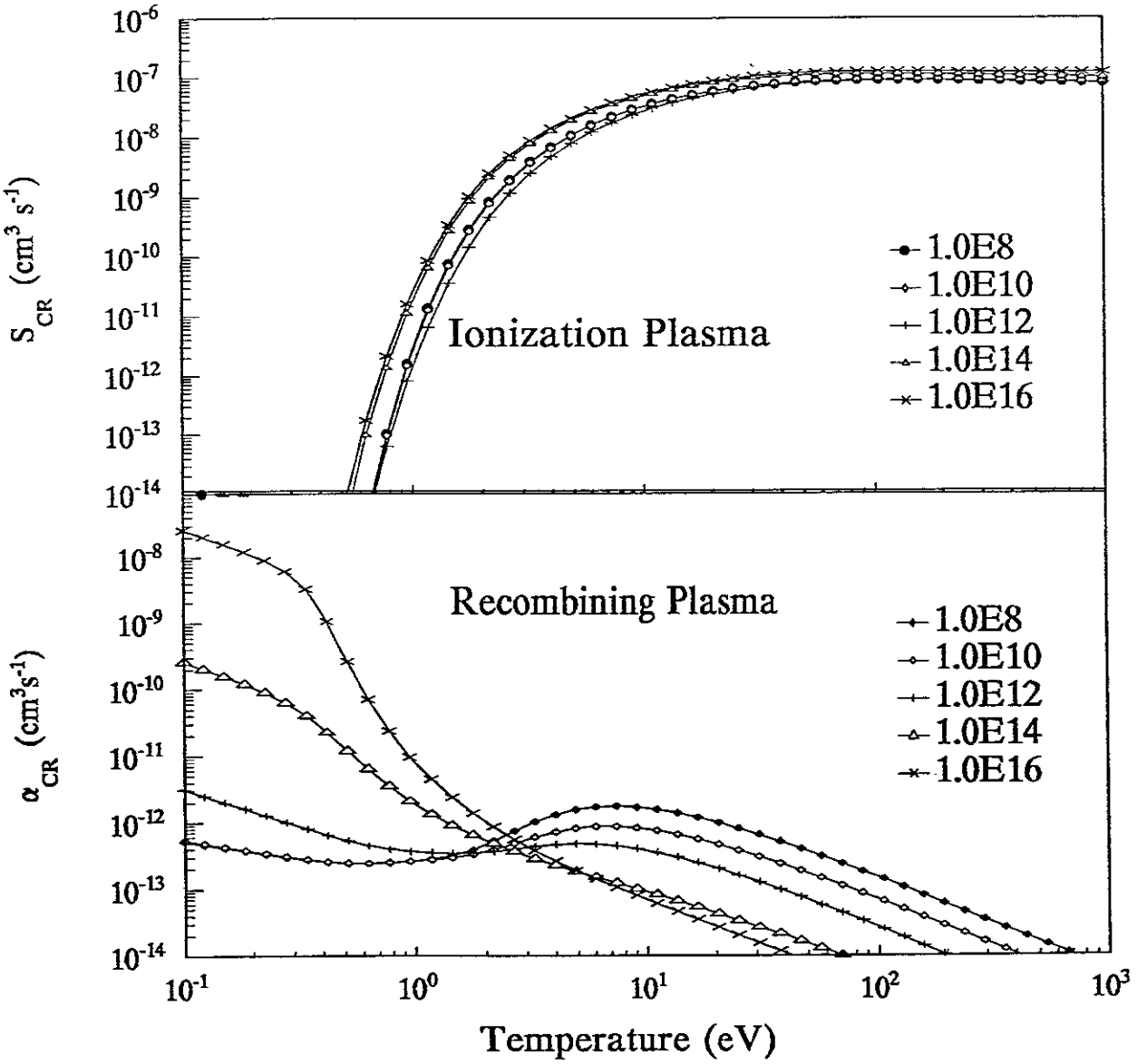

Fig.2 The collisional-radiative ionization rate coefficients (a) and collisional-radiative recombination rate coefficients (b) as a function of the elcectron temperature in different electron densities. All the units of electron densities are cm^{-3}.

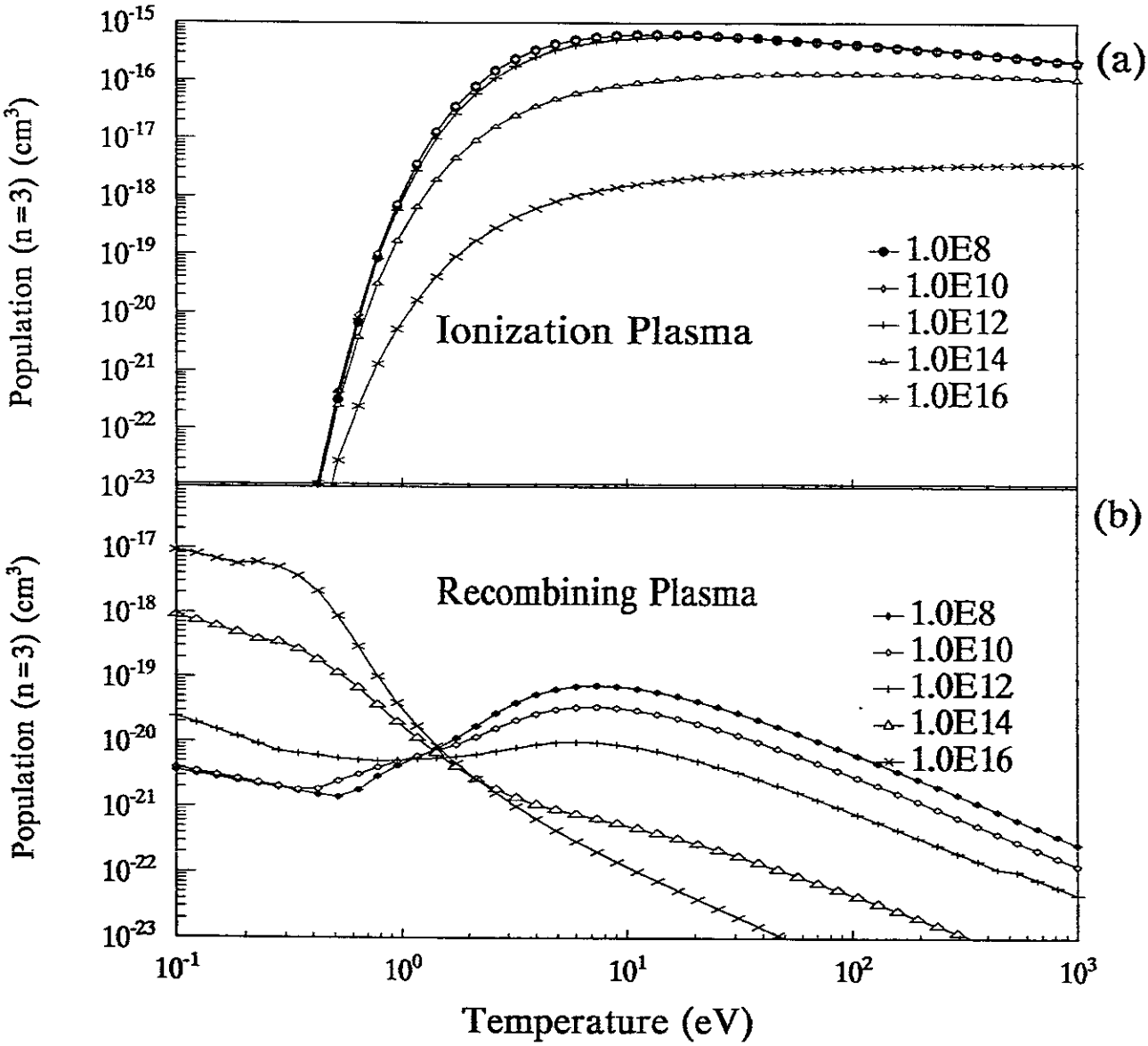

Fig.3 The total population for $2p3l$ as a function of the electron temperature in different eletron density. (a). Ionizing plasma; (b). Recombining plasma

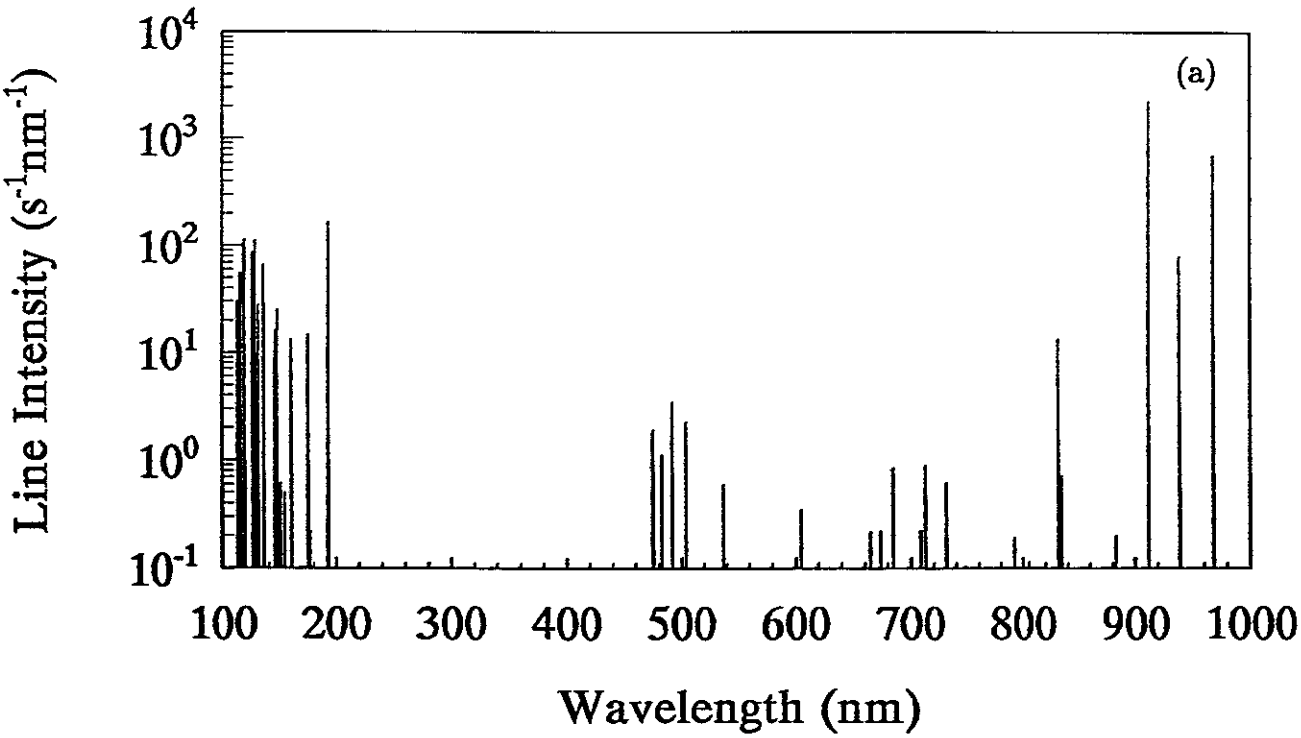

Fig.4 Spectra of neutral carbon at $T_e = 10eV$ and $n_e = 10^{10}cm^{-3}$ in the ionizing plasma. (a). wavelength: 100-1000 nm; (b). wavelength: 100-200 nm; (c). wavelength: 550-650 nm; (d). wavelength: 900-1000 nm.

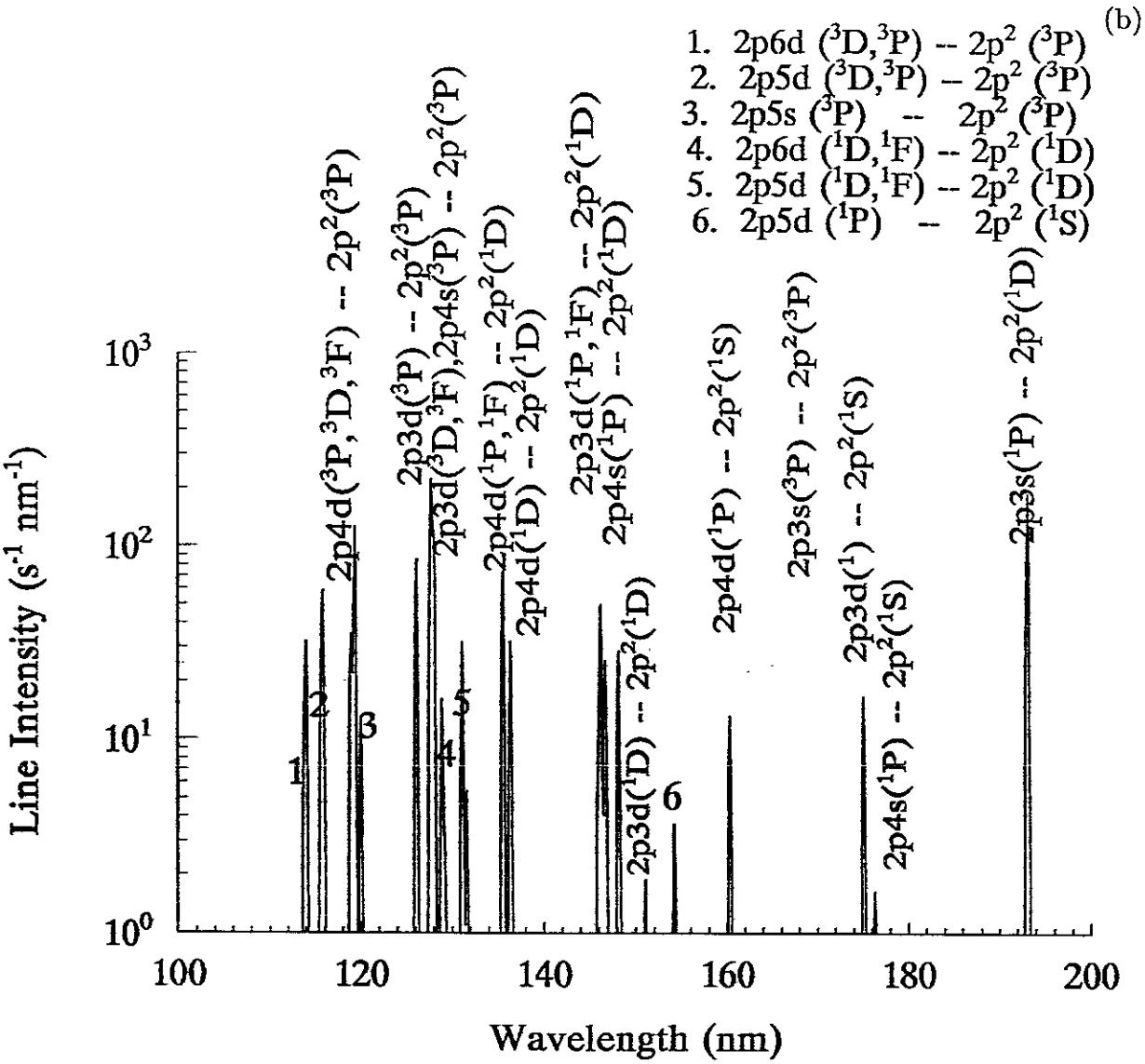
(b)
1. 2p6d (^{3}D,^{3}P) -- 2p^2 (^{3}P)
2. 2p5d (^{3}D,^{3}P) – 2p^2 (^{3}P)
3. 2p5s (^{3}P) -- 2p^2 (^{3}P)
4. 2p6d (^{1}D,^{1}F) -- 2p^2 (^{1}D)
5. 2p5d (^{1}D,^{1}F) -- 2p^2 (^{1}D)
6. 2p5d (^{1}P) -- 2p^2 (^{1}S)
Line Intensity (s^{-1} nm^{-1})
10^3
10^2
10^1
10^0
100
120
140
160
180
200
Wavelength (nm)
2p4d(^{3}P,^{3}D,^{3}F) -- 2p^2(^{3}P)
2p3d(^{3}P) -- 2p^2(^{3}P)
2p3d(^{3}D,^{3}F),2p4s(^{3}P) -- 2p^2(^{3}P)
2p4d(^{1}P,^{1}F) -- 2p^2(^{1}D)
2p4d(^{1}D) -- 2p^2(^{1}D)
2p3d(^{1}P,^{1}F) -- 2p^2(^{1}D)
2p4s(^{1}P) -- 2p^2(^{1}D)
2p3d(^{1}D) -- 2p^2(^{1}D)
2p4d(^{1}P) -- 2p^2(^{1}S)
2p3s(^{3}P) -- 2p^2(^{3}P)
2p3d(^{1}) -- 2p^2(^{1}S)
2p4s(^{1}P) -- 2p^2(^{1}S)
2p3s(^{1}P) -- 2p^2(^{1}D)

Fig.4

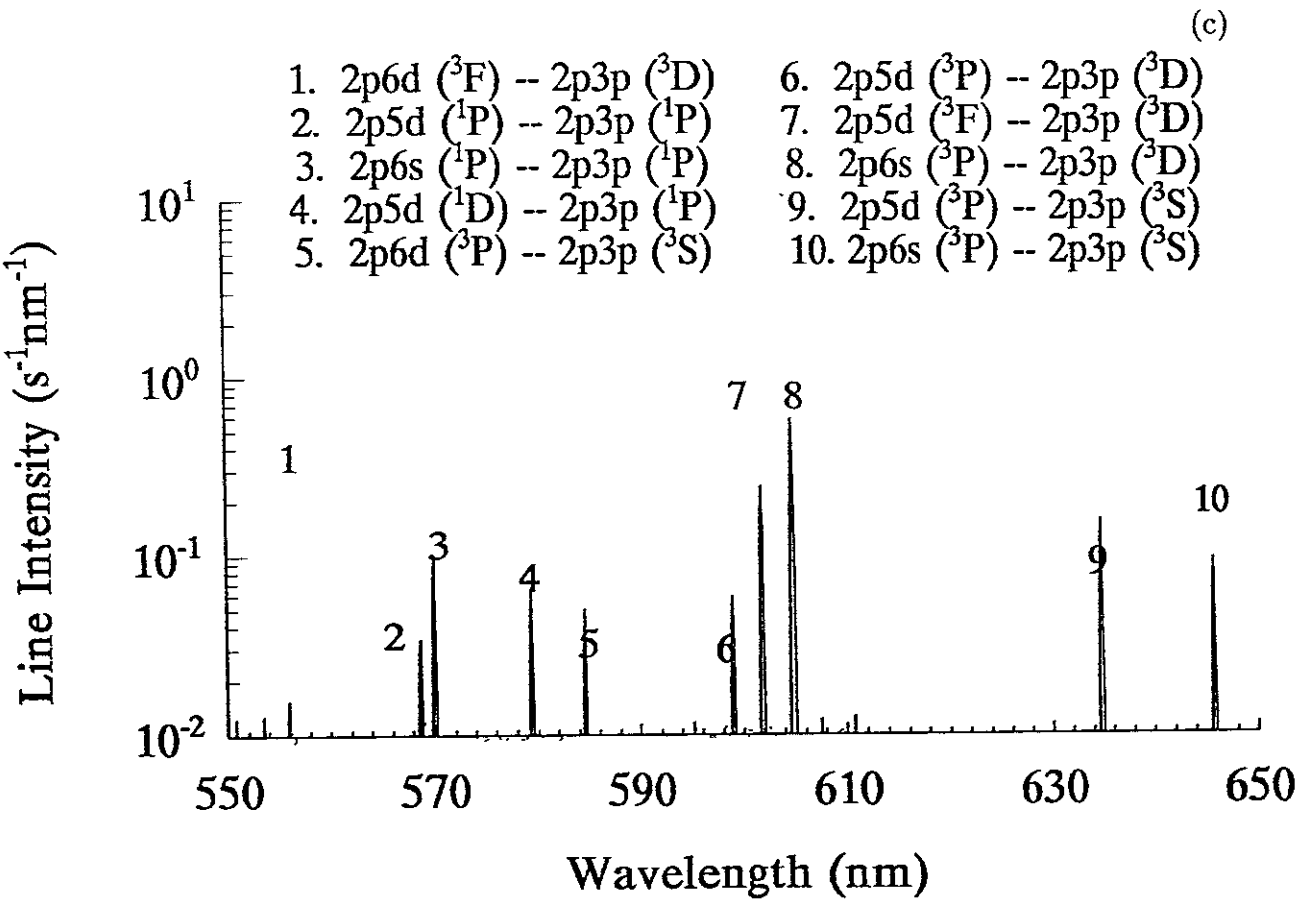
(c)
1. 2p6d (^{3}F) -- 2p3p (^{3}D)
2. 2p5d (^{1}P) -- 2p3p (^{1}P)
3. 2p6s (^{1}P) -- 2p3p (^{1}P)
4. 2p5d (^{1}D) -- 2p3p (^{1}P)
5. 2p6d (^{3}P) -- 2p3p (^{3}S)
6. 2p5d (^{3}P) -- 2p3p (^{3}D)
7. 2p5d (^{3}F) -- 2p3p (^{3}D)
8. 2p6s (^{3}P) -- 2p3p (^{3}D)
9. 2p5d (^{3}P) -- 2p3p (^{3}S)
10. 2p6s (^{3}P) -- 2p3p (^{3}S)
Line Intensity ($s^{-1}nm^{-1}$)
10^1
10^0
10^{-1}
10^{-2}
550
570
590
610
630
650
Wavelength (nm)

Fig.4

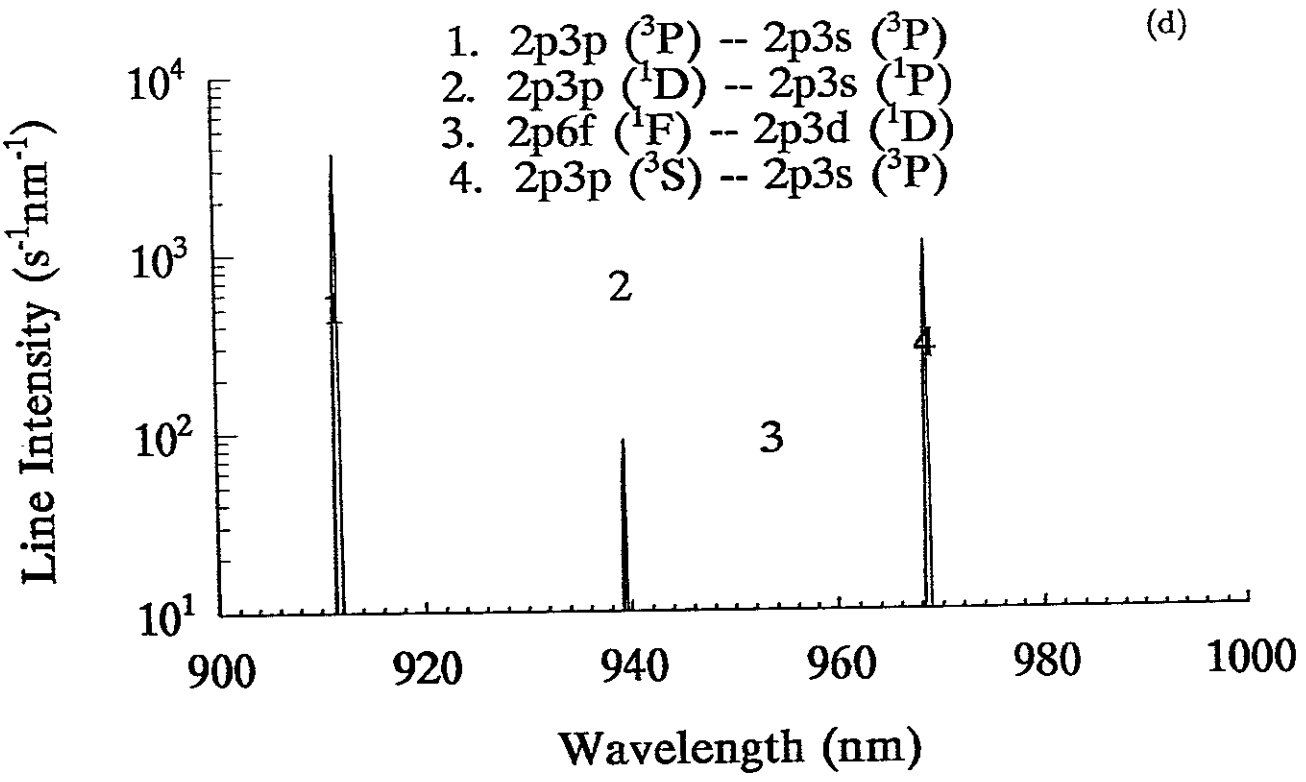
(d)
1. 2p3p (^{3}P) -- 2p3s (^{3}P)
2. 2p3p (^{1}D) -- 2p3s (^{1}P)
3. 2p6f (^{1}F) -- 2p3d (^{1}D)
4. 2p3p (^{3}S) -- 2p3s (^{3}P)
Line Intensity ($s^{-1}nm^{-1}$)
10^4
10^3
10^2
10^1
900
920
940
960
980
1000
Wavelength (nm)

Fig.4

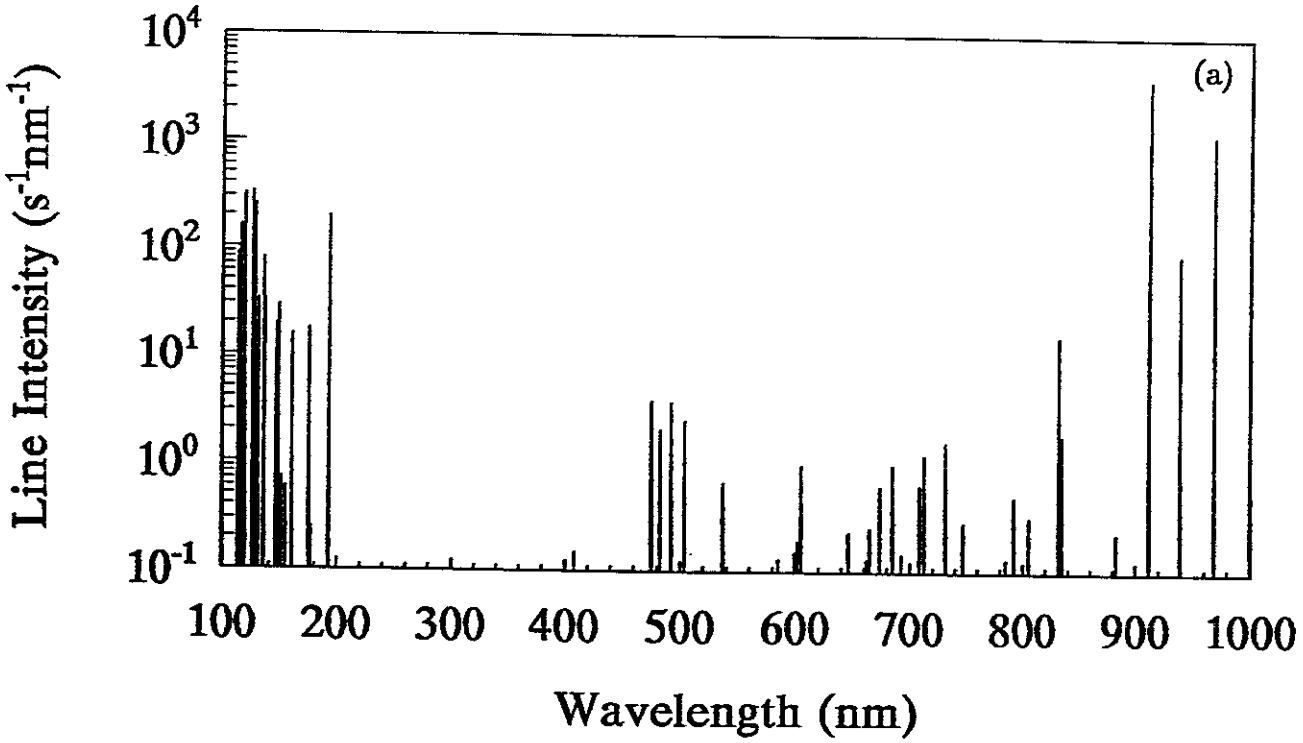

Fig.5 Spectra of neutral carbon at $T_e = 100eV$ and $n_e = 10^{10}cm^{-3}$ in the ionizing plasma. (a). wavelength: 100-1000 nm; (b). wavelength: 100-200 nm; (c). wavelength: 550-650 nm; (d). wavelength: 900-1000 nm.

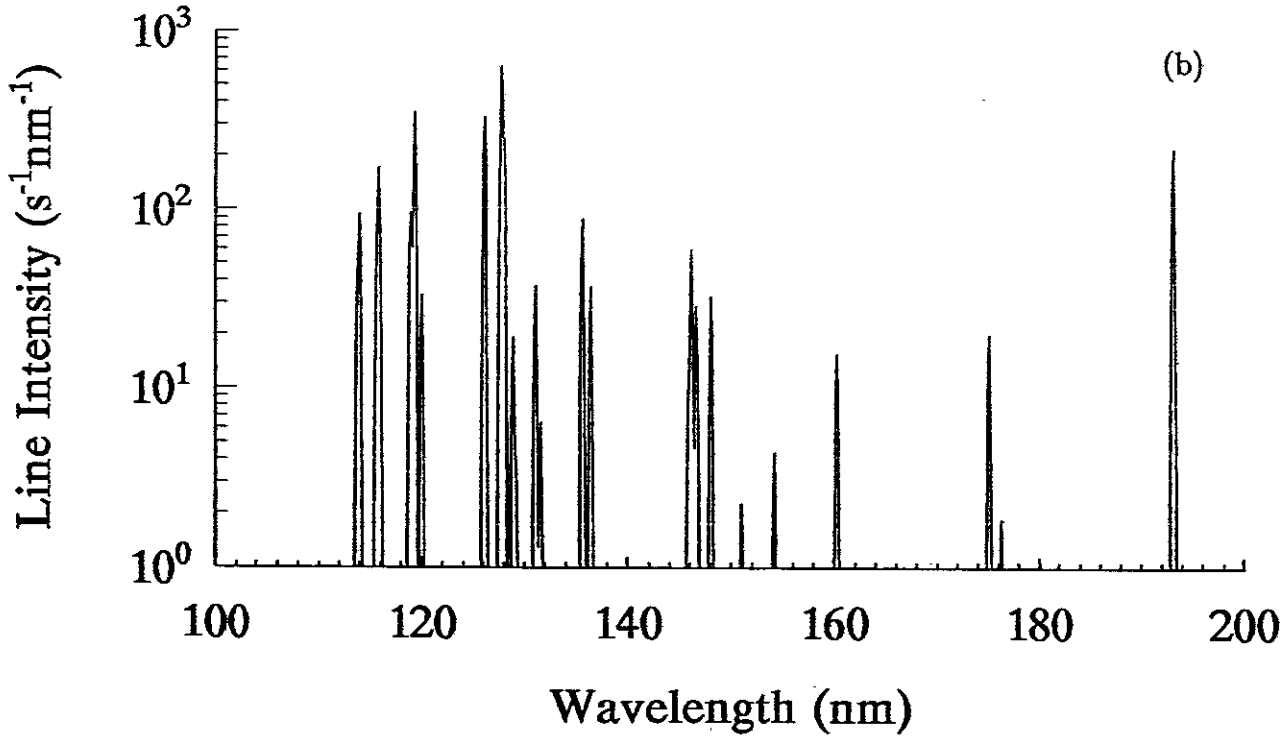

Fig.5

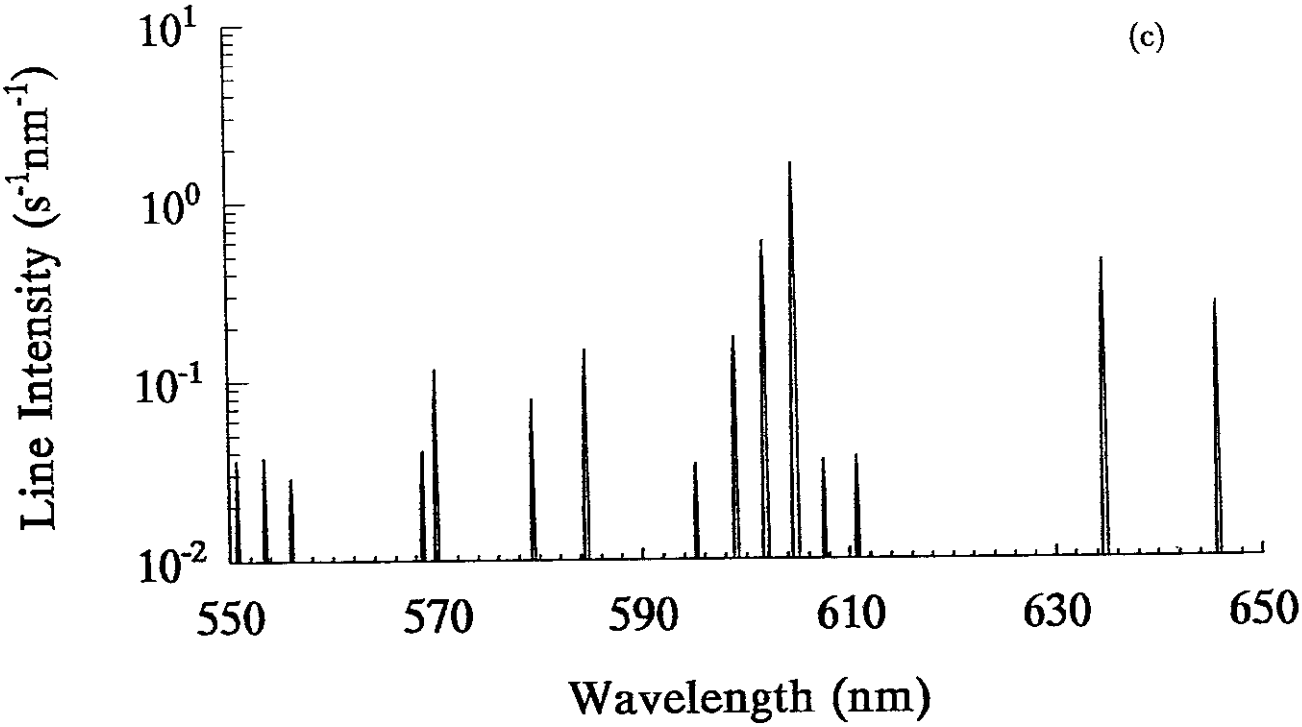
(c)
Line Intensity ($s^{-1}nm^{-1}$)
10^{1}
10^{0}
10^{-1}
10^{-2}
550
570
590
610
630
650
Wavelength (nm)

Fig.5

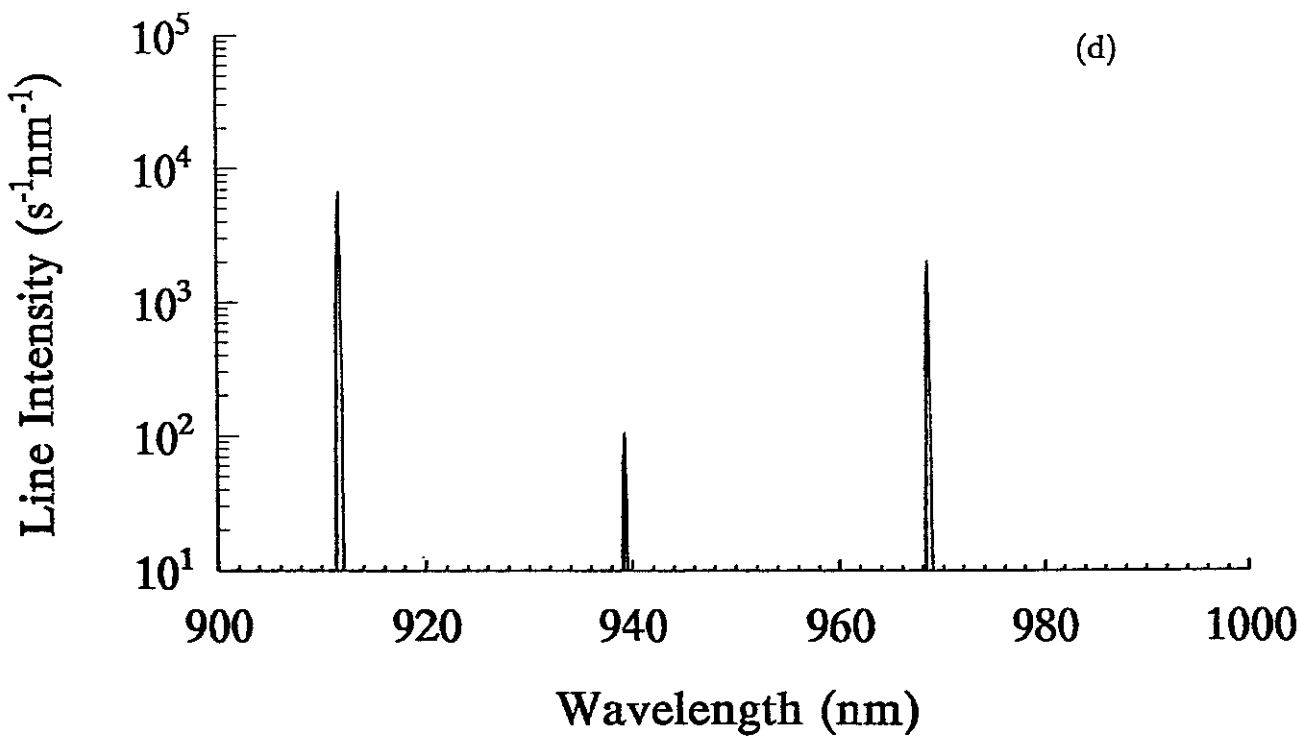
(d)
Line Intensity ($s^{-1}nm^{-1}$)
10^{5}
10^{4}
10^{3}
10^{2}
10^{1}
900
920
940
960
980
1000
Wavelength (nm)

Fig.5

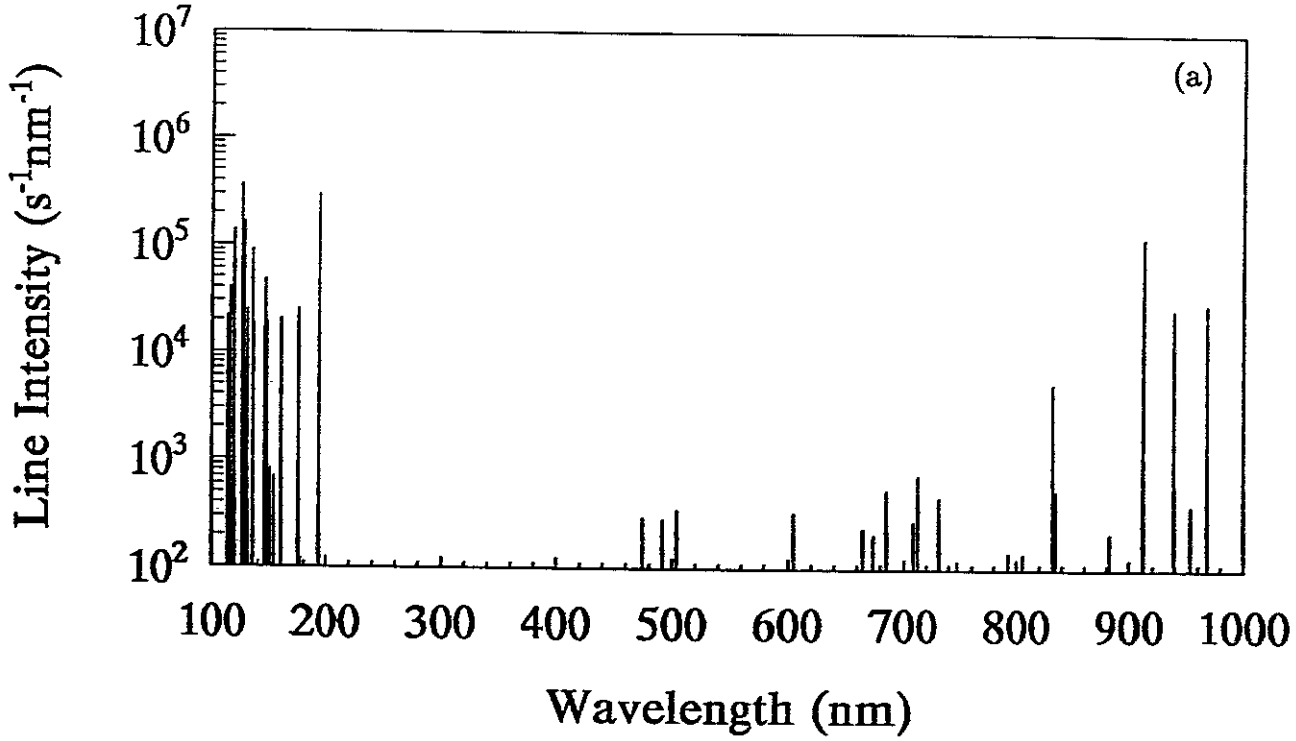

Fig.6 Spectra of neutral carbon at $T_e = 10eV$ and $n_e = 10^{14}cm^{-3}$ in the ionizing plasma. (a). wavelength: 100-1000 nm; (b). wavelength: 100-200 nm; (c). wavelength: 550-650 nm; (d). wavelength: 900-1000 nm.

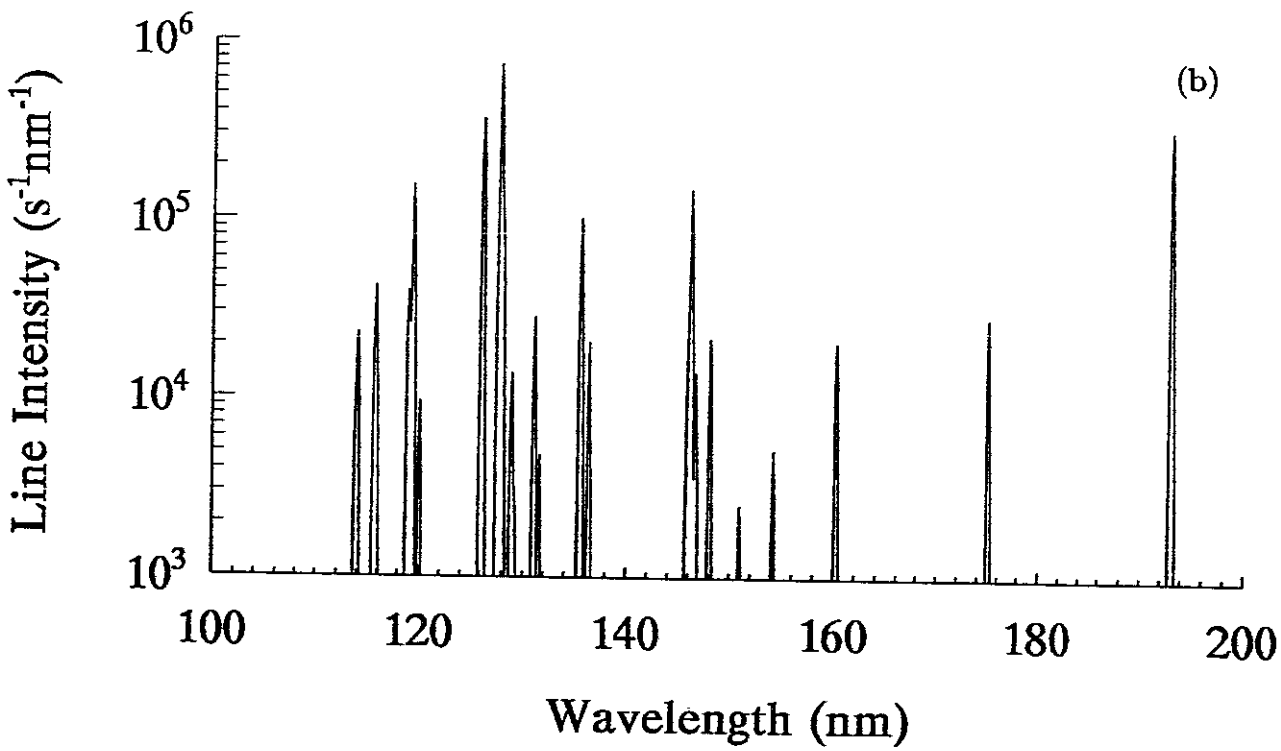

Fig.6

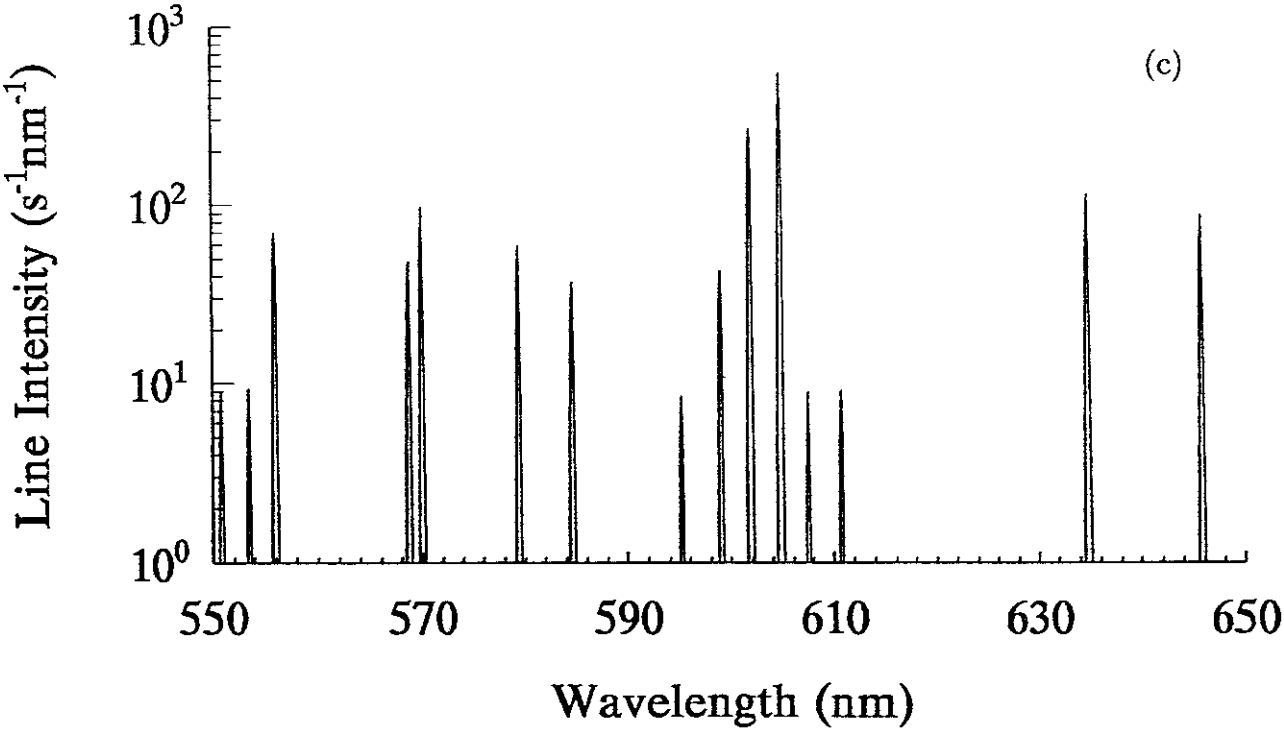
(c)
Line Intensity ($s^{-1}nm^{-1}$)
10^3
10^2
10^1
10^0
550
570
590
610
630
650
Wavelength (nm)

Fig.6

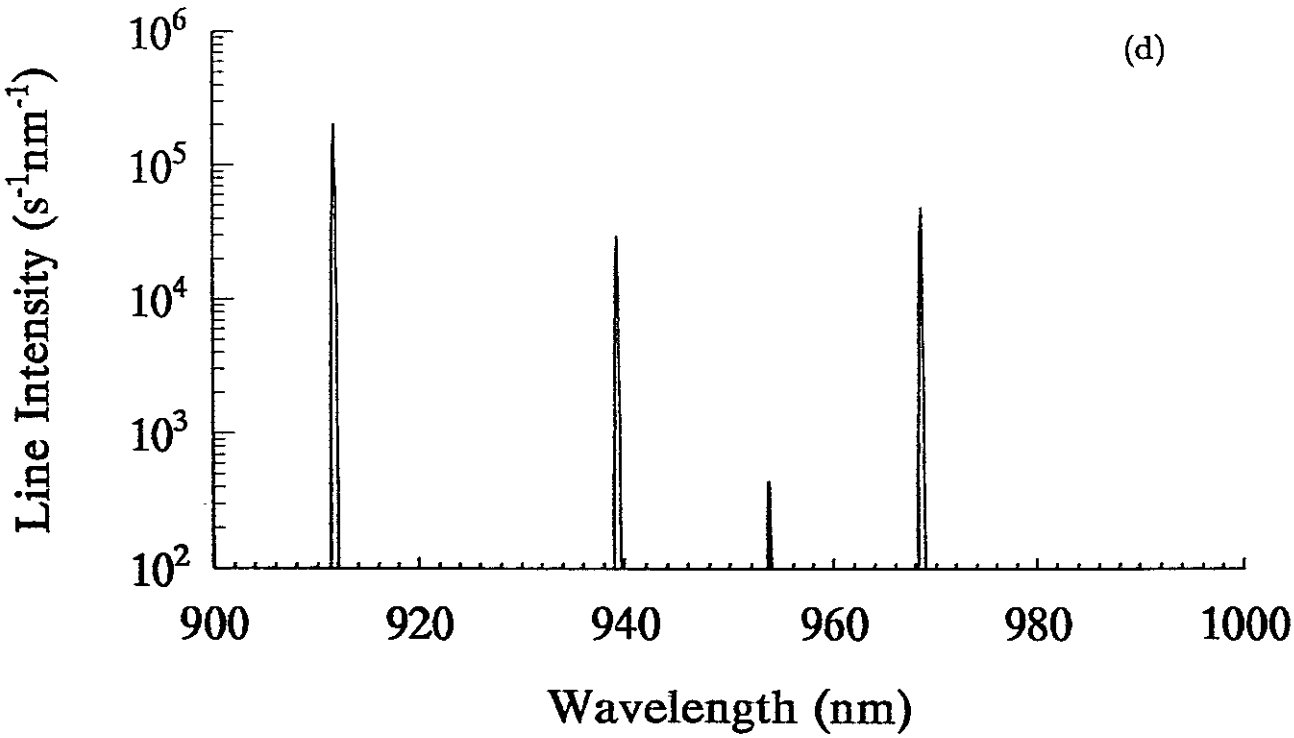
(d)
Line Intensity ($s^{-1}nm^{-1}$)
10^6
10^5
10^4
10^3
10^2
900
920
940
960
980
1000
Wavelength (nm)

Fig.6

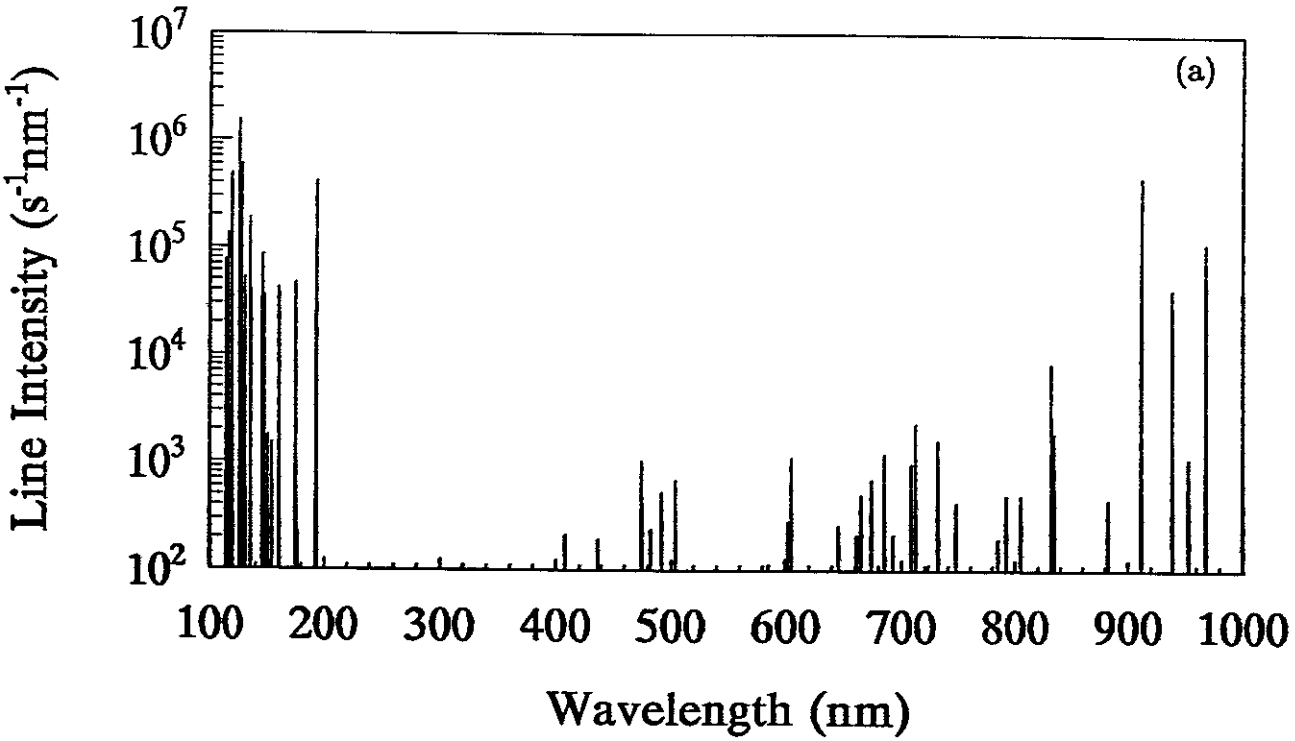

Fig.7 Spectra of neutral carbon at $T_e = 100eV$ and $n_e = 10^{14}cm^{-3}$ in the ionizing plasma. (a). wavelength: 100-1000 nm; (b). wavelength: 100-200 nm; (c). wavelength: 550-650 nm; (d). wavelength: 900-1000 nm.

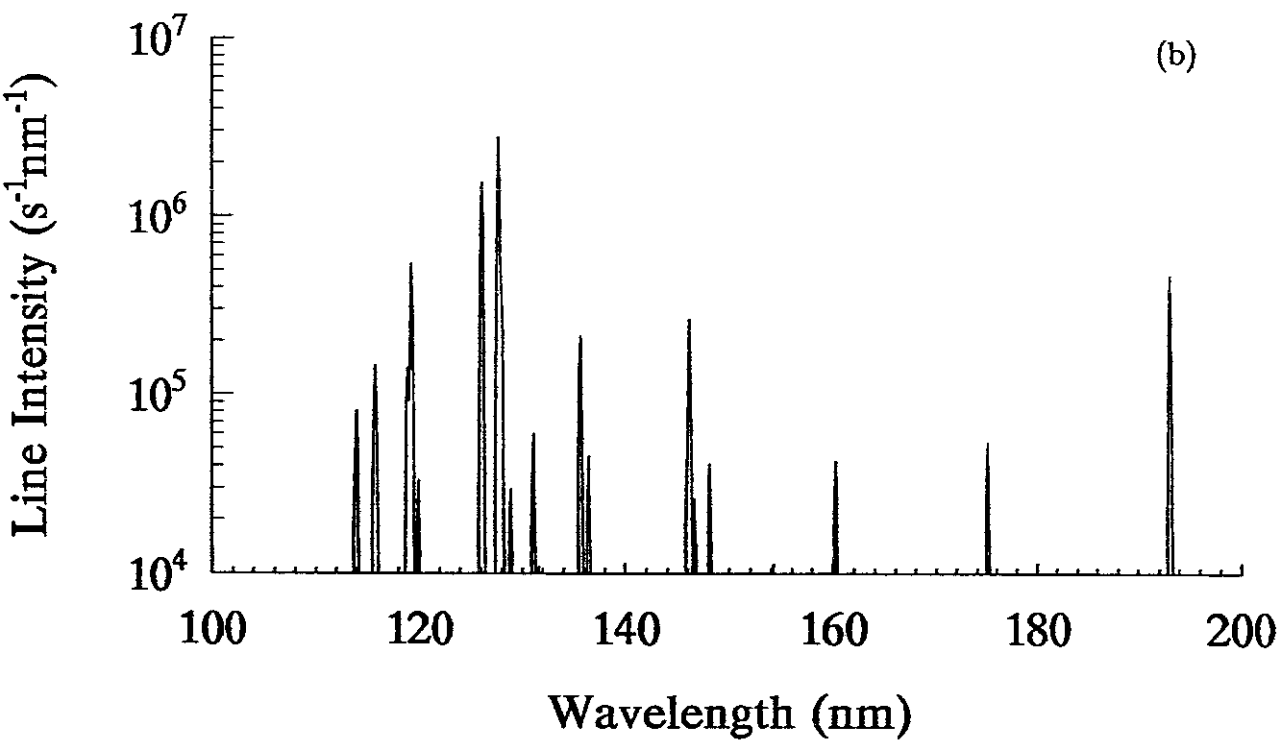

Fig.7

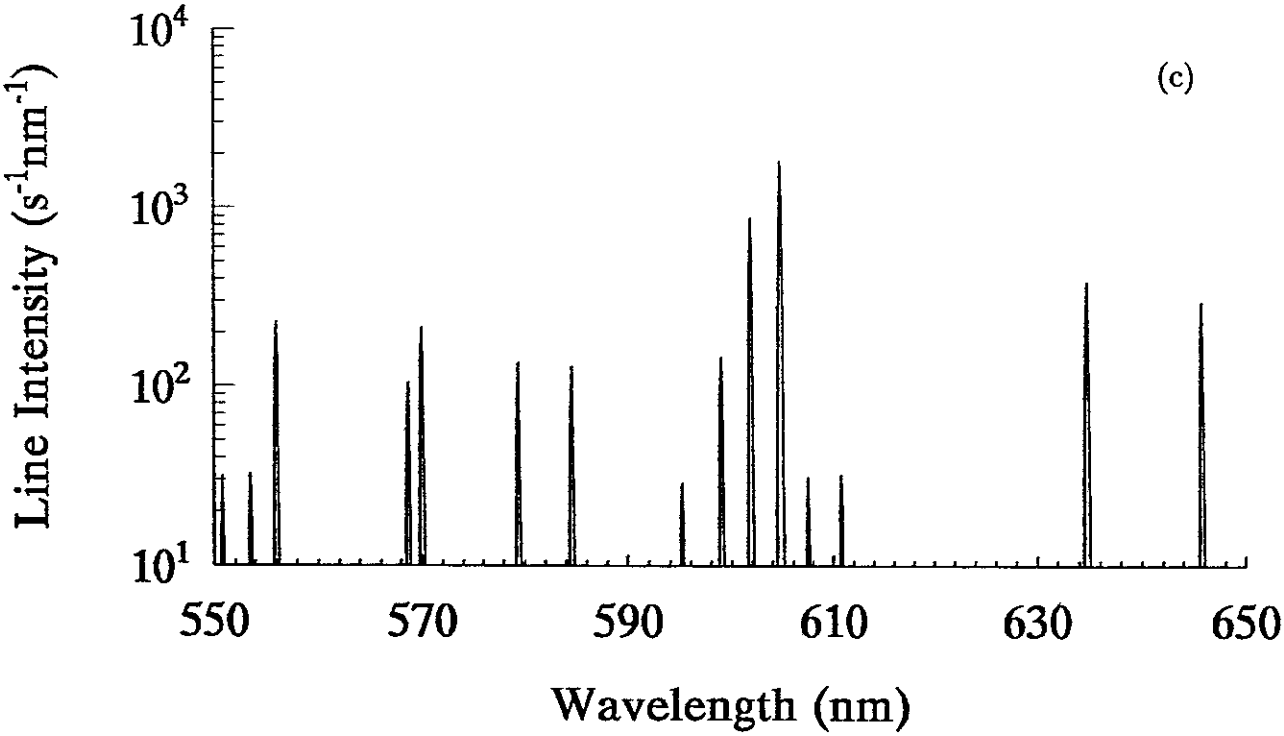
(c)
Line Intensity ($s^{-1}nm^{-1}$)
10^4
10^3
10^2
10^1
550
570
590
610
630
650
Wavelength (nm)

Fig.7

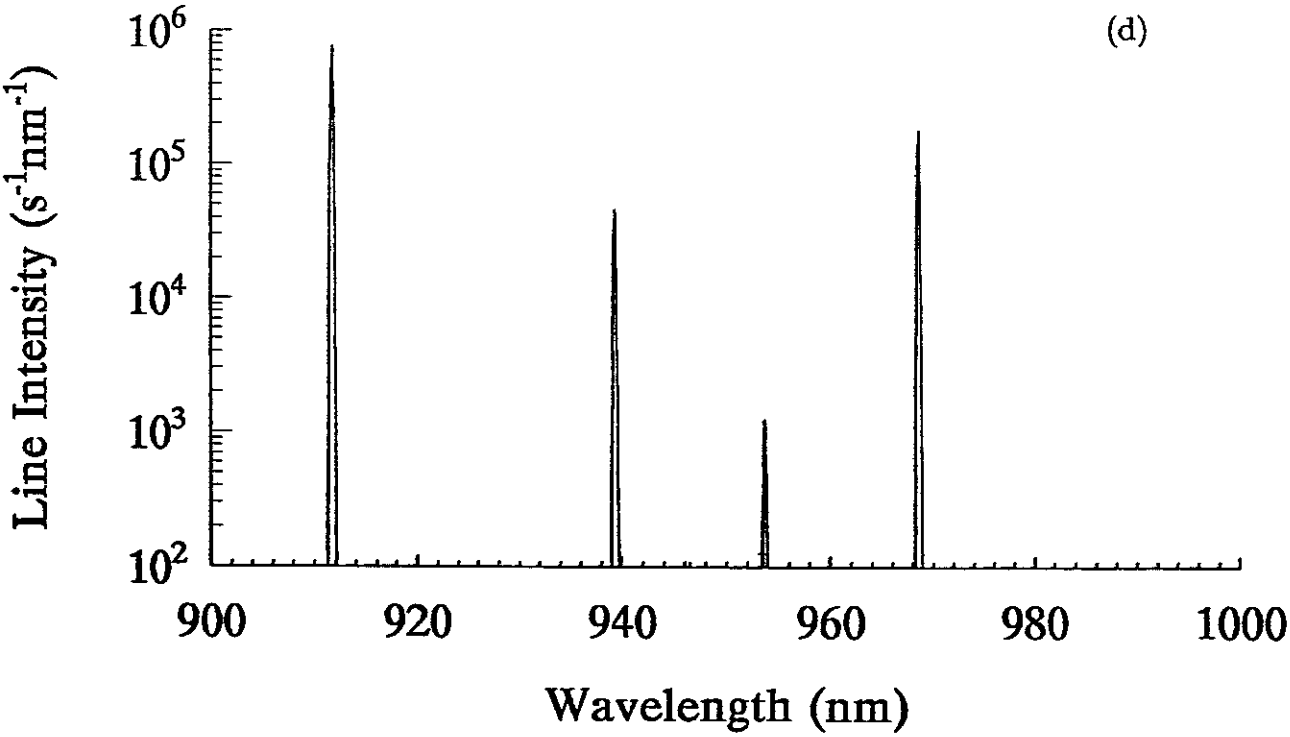
(d)
Line Intensity ($s^{-1}nm^{-1}$)
10^6
10^5
10^4
10^3
10^2
900
920
940
960
980
1000
Wavelength (nm)

Fig.7

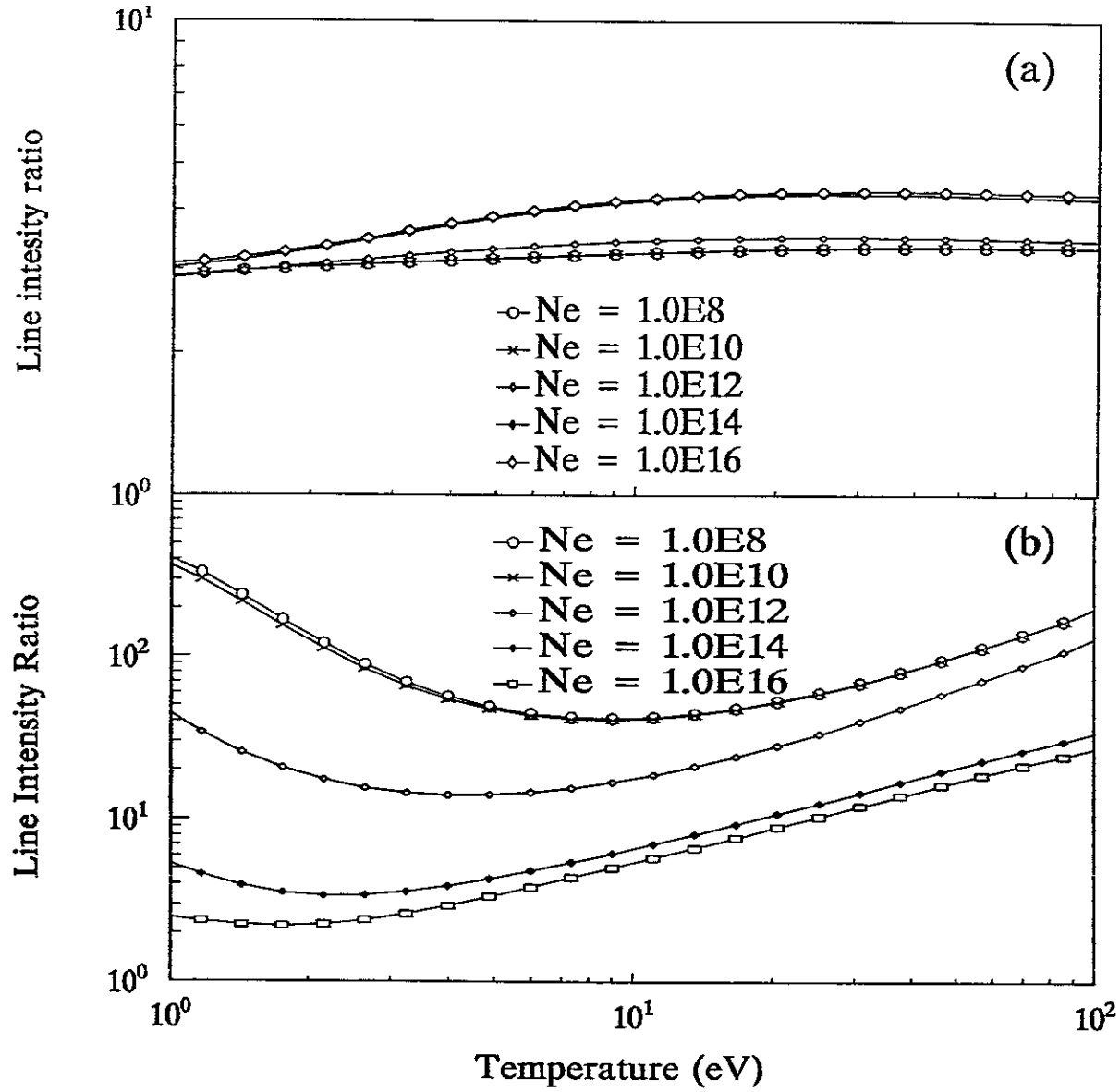

Fig.8 Line intensity ratio as a function of the electron temperature in the ionizing plasma. (a). 912 nm ($2p3p(^3P) \rightarrow 2p3s(^3P)$)/968 nm ($2p3p(^3S) \rightarrow 2p3s(^3P)$); (b). 912 nm ($2p3p(^3P) \rightarrow 2p3s(^3P)$)/939 nm ($2p3p(^1D) \rightarrow 2p3s(^1P)$)

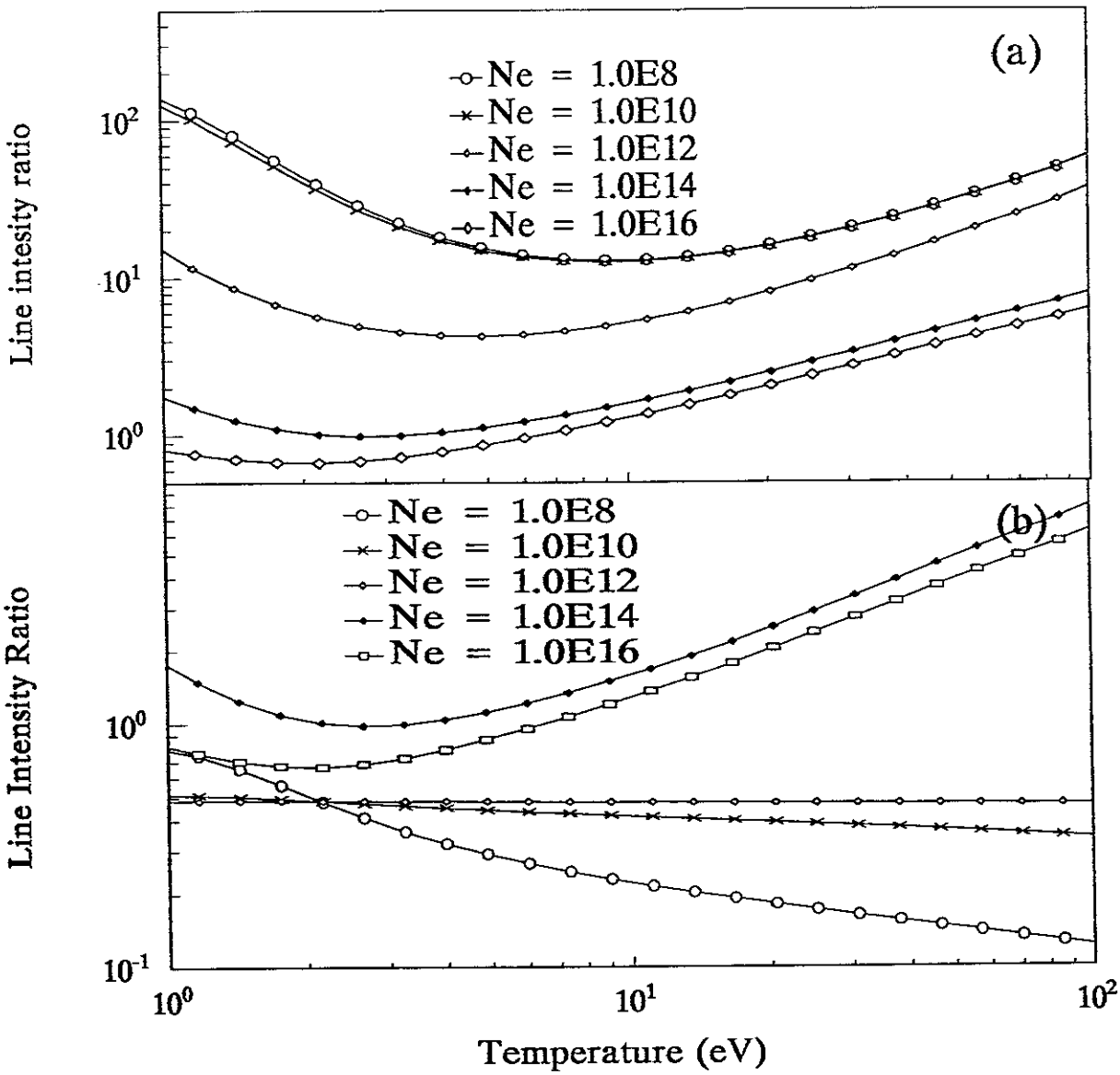

Fig.9 Line intensity ratio as a function of the electron temperature in the ionizing plasma. (a). 968 nm ($2p3p(^3S) \rightarrow 2p3s(^3P)$) /939 nm ($2p3p(^1D) \rightarrow 2p3s(^1P)$) (b). 602 nm ($2p5d(^3F) \rightarrow 2p3p(^3D)$) /605 nm ($2p6s(^3P) \rightarrow 2p3p(^3D)$)

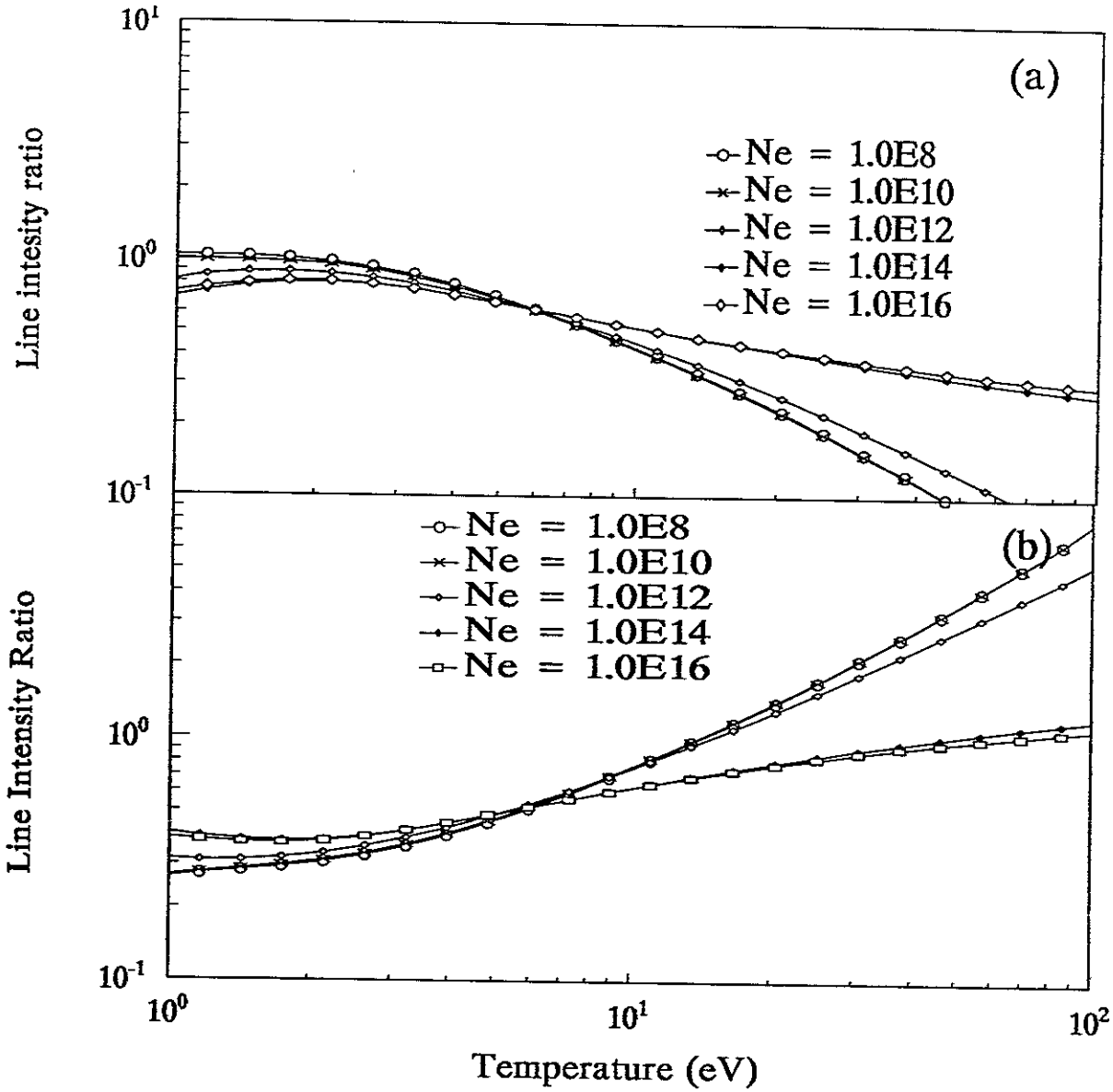

Fig.10 Line intensity ratio as a function of the electron temperature in the ionizing plasma. (a). 579 nm ($2p5d(^1D) \rightarrow 2p3p(^1P)$) /635 nm ($2p5d(^3P) \rightarrow 2p3p(^3S)$) (b). 585 nm ($2p6d(^3P) \rightarrow 2p3p(^3S)$) /579 nm ($2p5d(^1D) \rightarrow 2p3p(^1P)$)

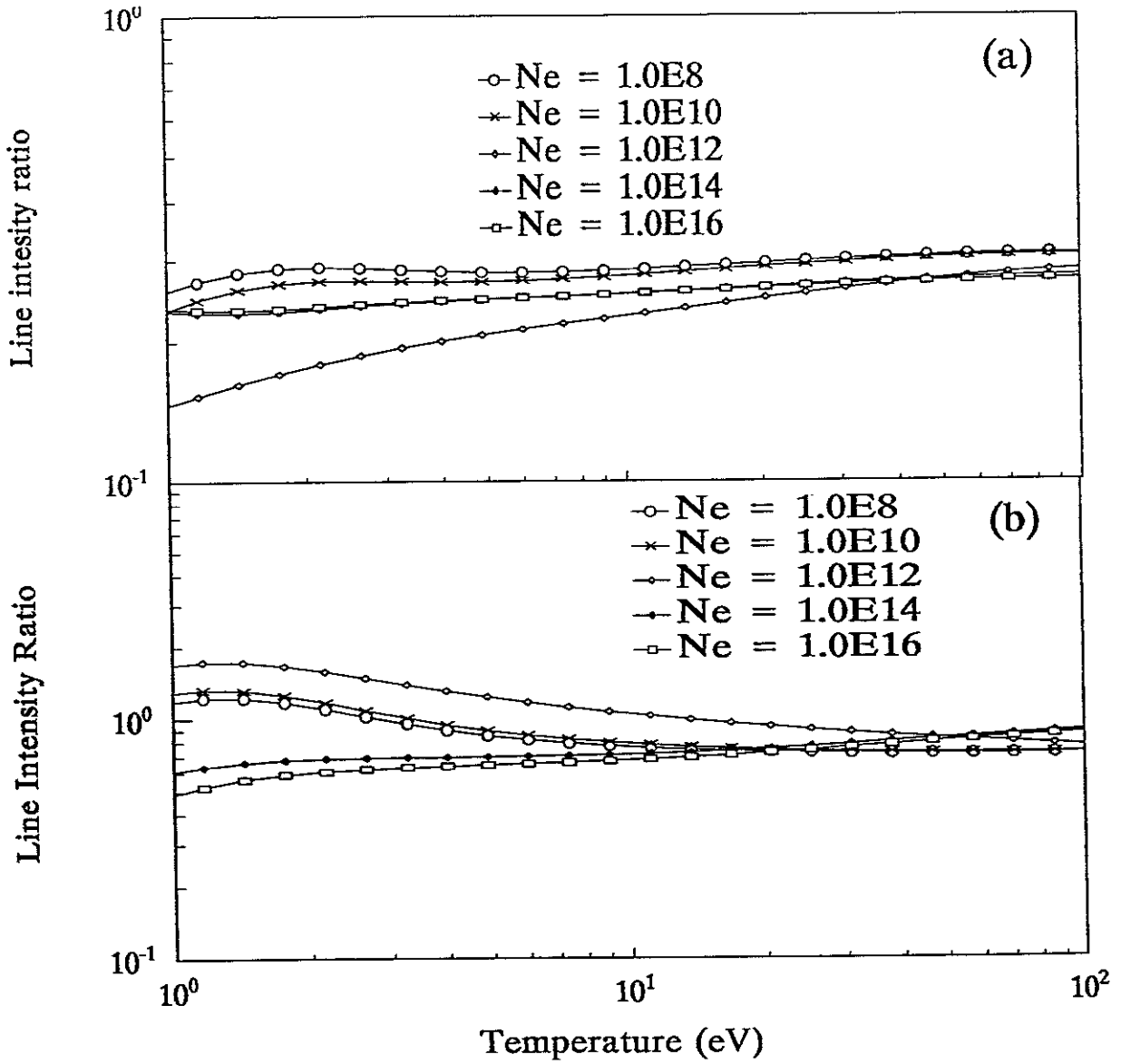

Fig.11 Line intensity ratio as a function of the electron temperature in the ionizing plasma. (a). 156 nm ($2p5d(^1P) \rightarrow 2p^2(^1S)$) /160 nm ($2p4d(^1P) \rightarrow 2p^2(^1S)$) (b). 160 nm ($2p4d(^1P) \rightarrow 2p^2(^1S)$) /175 nm ($2p3d(^1P) \rightarrow 2p^2(^1S)$)

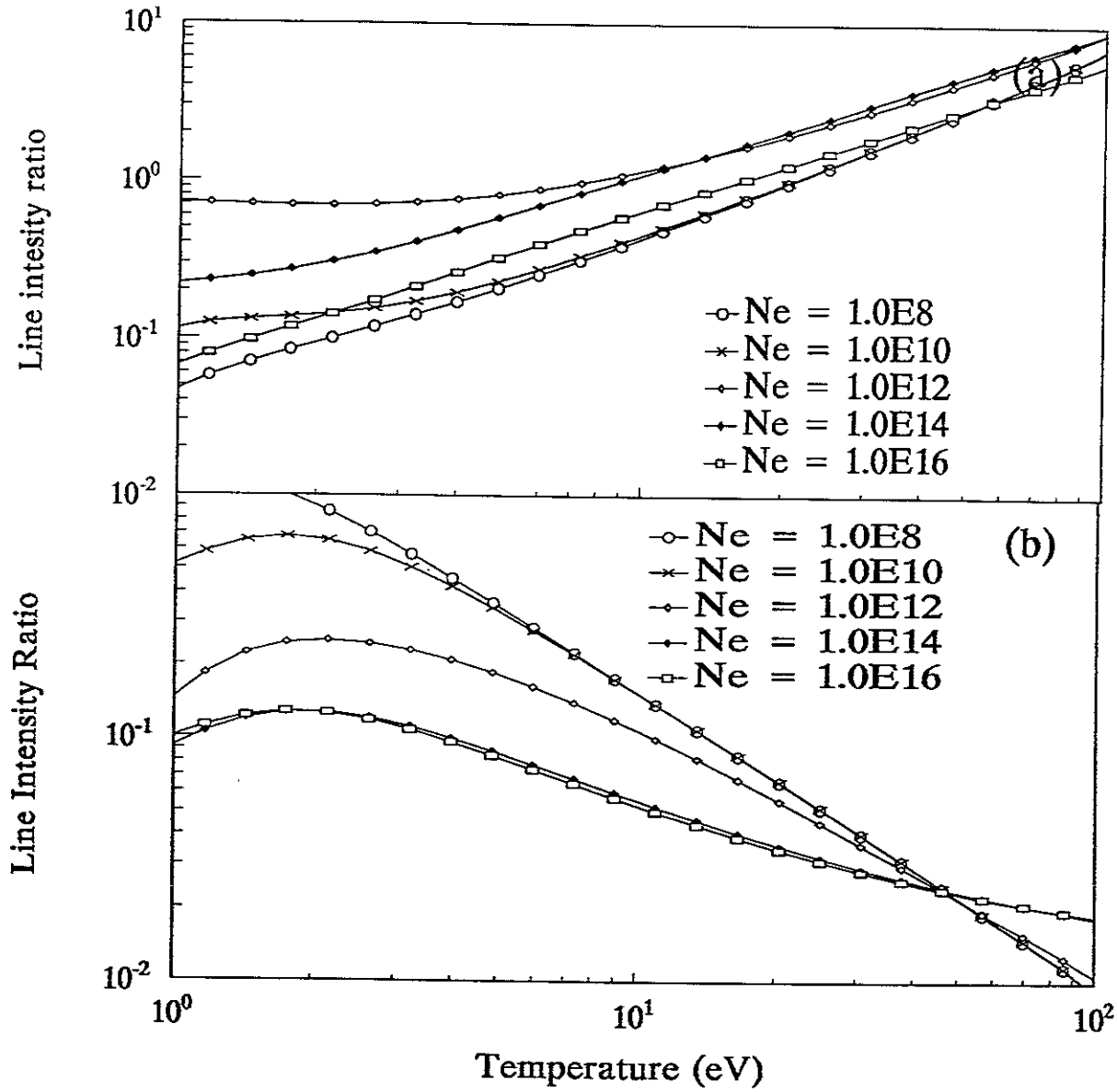

Fig.12 Line intensity ratio as a function of the electron temperature in the ionizing plasma. (a). 126 nm ($2p3d(^3P) \rightarrow 2p^2(^3P)$) /193 nm ($2p3s(^1P) \rightarrow 2p^2(^1D)$) (b). 160 nm ($2p4d(^1P) \rightarrow 2p^2(^1S)$) /126 nm ($2p3d(^3P) \rightarrow 2p^2(^3P)$)

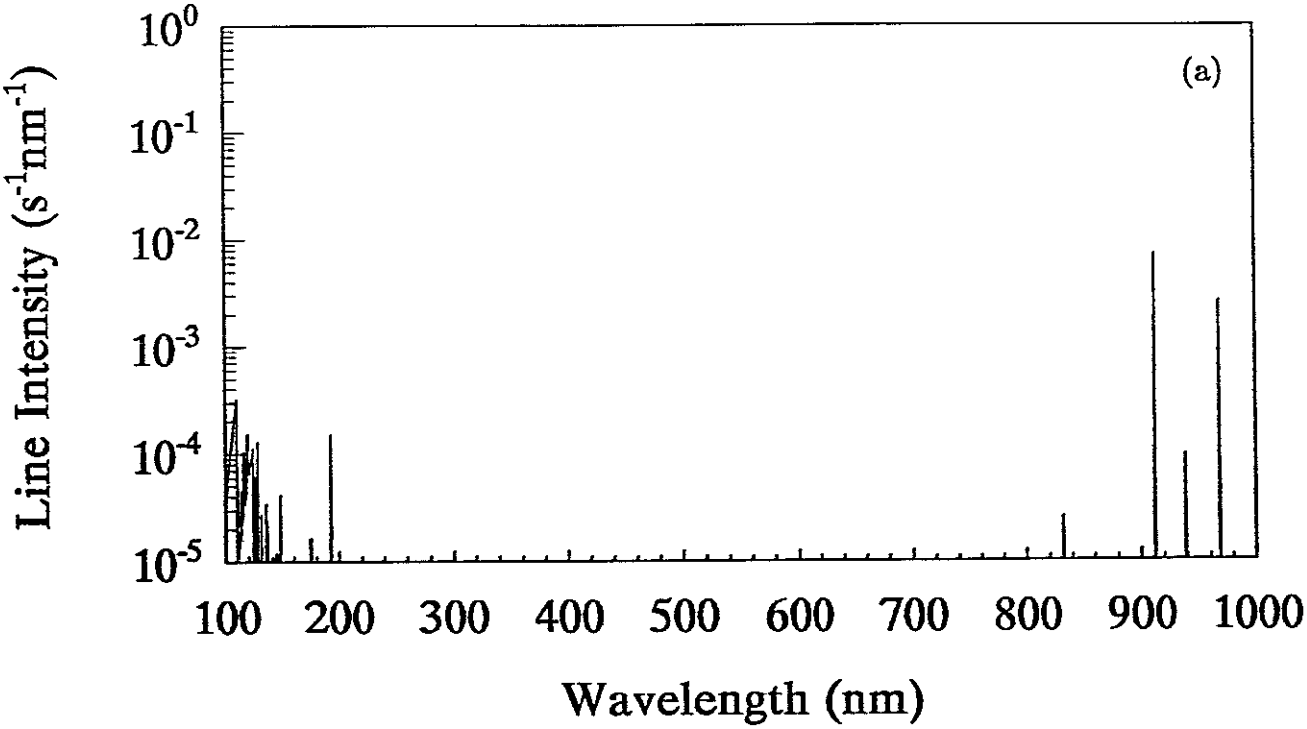

Fig.13 Spectra of neutral carbon at $T_e = 0.5eV$ and $n_e = 10^{10}cm^{-3}$ in the recombining plasma. (a). wavelength: 100-1000 nm; (b). wavelength: 100-200 nm; (c). wavelength: 550-650 nm; (d). wavelength: 900-1000 nm.

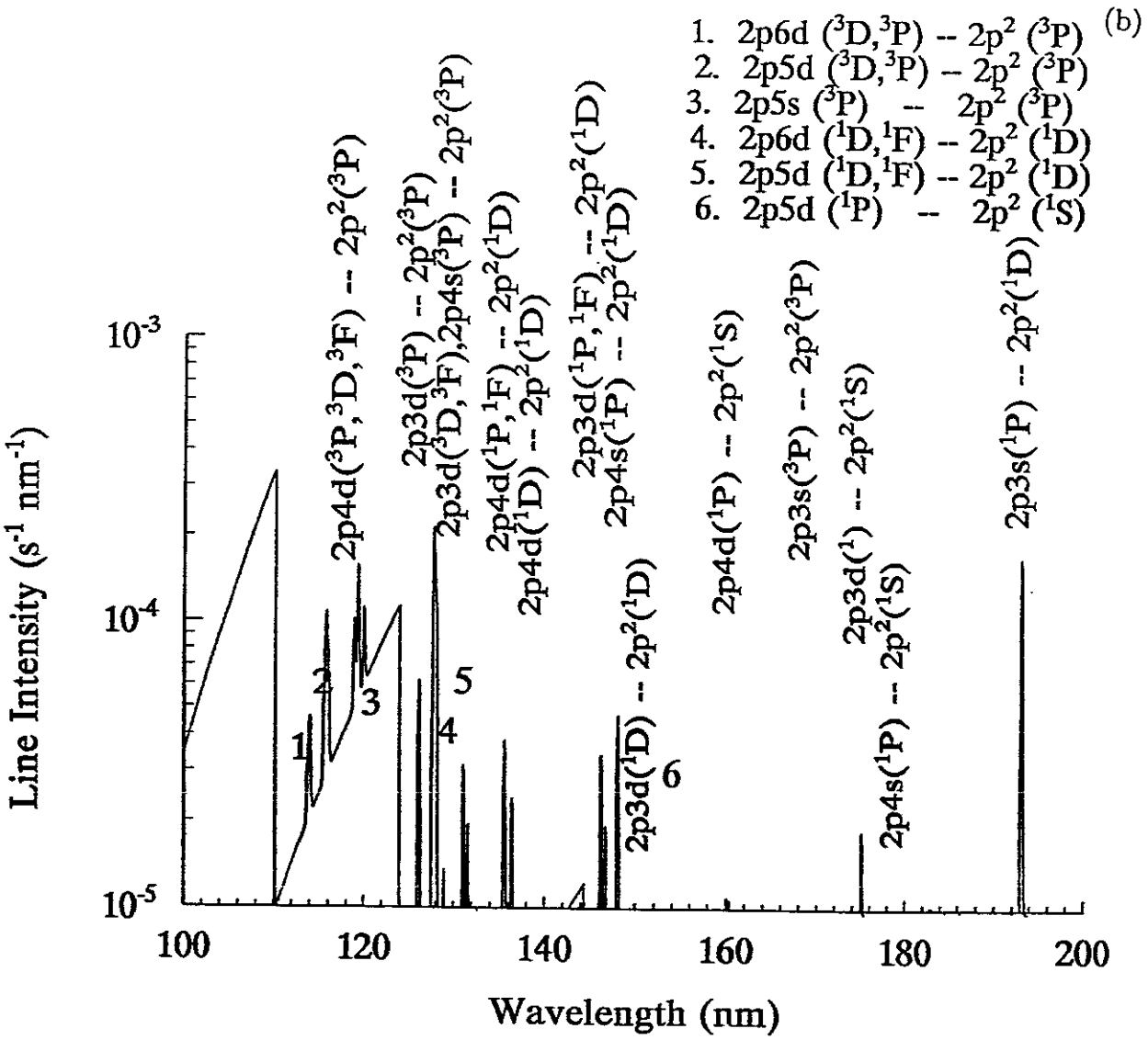
(b)
1. 2p6d (^{3}D,^{3}P) -- 2p^2 (^{3}P)
2. 2p5d (^{3}D,^{3}P) -- 2p^2 (^{3}P)
3. 2p5s (^{3}P) -- 2p^2 (^{3}P)
4. 2p6d (^{1}D,^{1}F) -- 2p^2 (^{1}D)
5. 2p5d (^{1}D,^{1}F) -- 2p^2 (^{1}D)
6. 2p5d (^{1}P) -- 2p^2 (^{1}S)
Line Intensity (s^{-1} nm^{-1})
10^{-3}
10^{-4}
10^{-5}
100
120
140
160
180
200
Wavelength (nm)
2p4d(^{3}P,^{3}D,^{3}F) -- 2p^2(^{3}P)
2p3d(^{3}P) -- 2p^2(^{3}P)
2p3d(^{3}D,^{3}F),2p4s(^{3}P) -- 2p^2(^{3}P)
2p4d(^{1}P,^{1}F) -- 2p^2(^{1}D)
2p4d(^{1}D) -- 2p^2(^{1}D)
2p3d(^{1}P,^{1}F) -- 2p^2(^{1}D)
2p4s(^{1}P) -- 2p^2(^{1}D)
2p3d(^{1}D) -- 2p^2(^{1}D)
2p4d(^{1}P) -- 2p^2(^{1}S)
2p3s(^{3}P) -- 2p^2(^{3}P)
2p3d(^{1}) -- 2p^2(^{1}S)
2p4s(^{1}P) -- 2p^2(^{1}S)
2p3s(^{1}P) -- 2p^2(^{1}D)
1
2
3
4
5
6

Fig.13

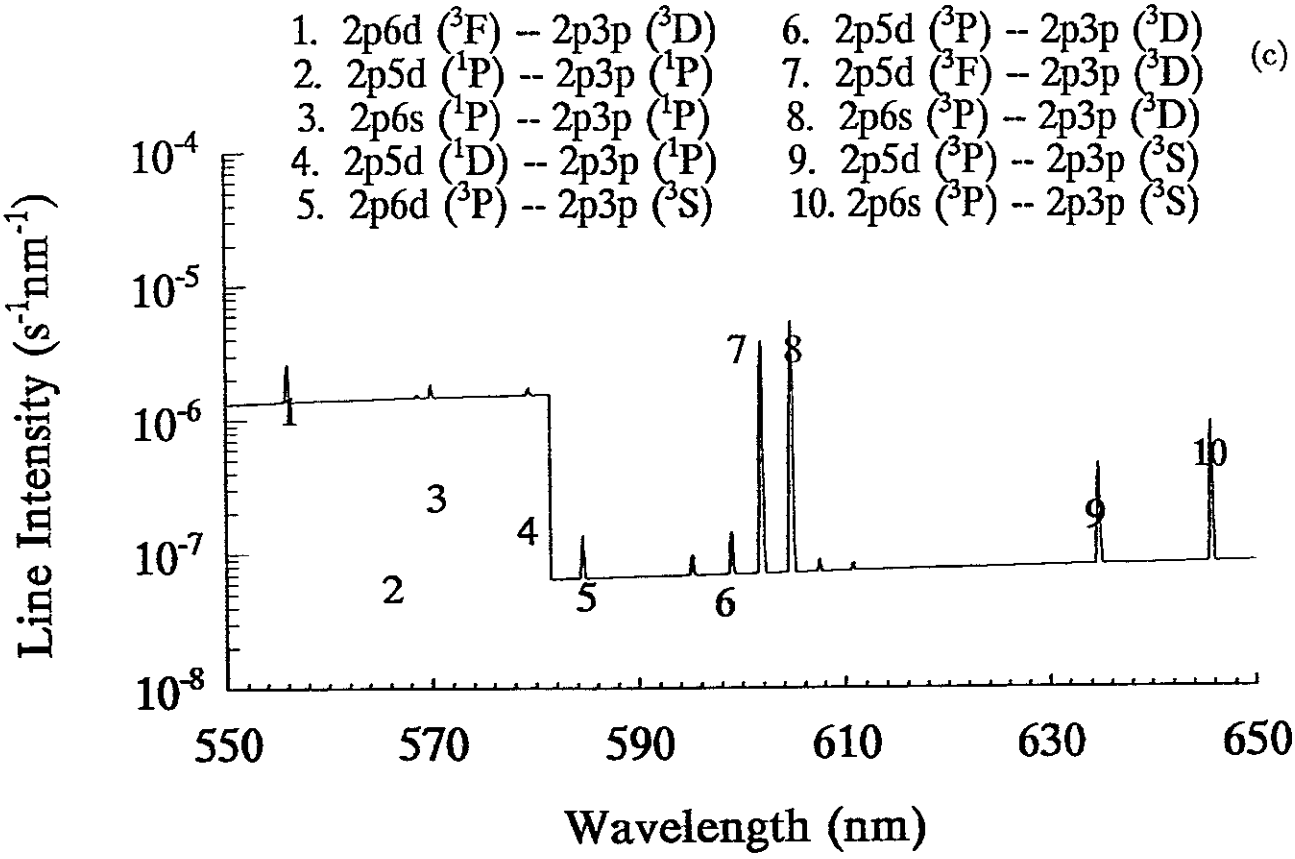
1. 2p6d (^{3}F) -- 2p3p (^{3}D)
2. 2p5d (^{1}P) -- 2p3p (^{1}P)
3. 2p6s (^{1}P) -- 2p3p (^{1}P)
4. 2p5d (^{1}D) -- 2p3p (^{1}P)
5. 2p6d (^{3}P) -- 2p3p (^{3}S)
6. 2p5d (^{3}P) -- 2p3p (^{3}D)
7. 2p5d (^{3}F) -- 2p3p (^{3}D)
8. 2p6s (^{3}P) -- 2p3p (^{3}D)
9. 2p5d (^{3}P) -- 2p3p (^{3}S)
10. 2p6s (^{3}P) -- 2p3p (^{3}S)
(c)
Line Intensity ($s^{-1}nm^{-1}$)
10^{-4}
10^{-5}
10^{-6}
10^{-7}
10^{-8}
550
570
590
610
630
650
Wavelength (nm)

Fig.13

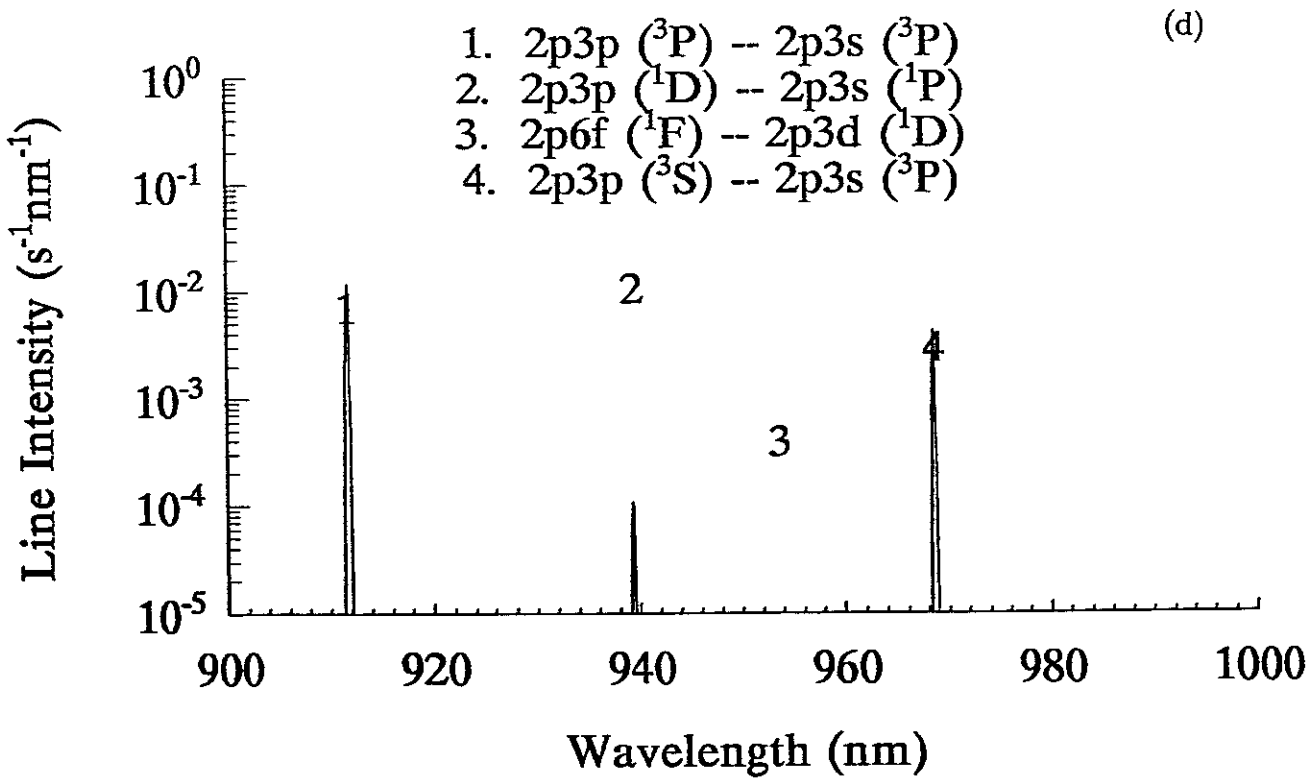
1. 2p3p (^{3}P) -- 2p3s (^{3}P)
2. 2p3p (^{1}D) -- 2p3s (^{1}P)
3. 2p6f (^{1}F) -- 2p3d (^{1}D)
4. 2p3p (^{3}S) -- 2p3s (^{3}P)
(d)
Line Intensity ($s^{-1}nm^{-1}$)
10^{0}
10^{-1}
10^{-2}
10^{-3}
10^{-4}
10^{-5}
900
920
940
960
980
1000
Wavelength (nm)

Fig.13

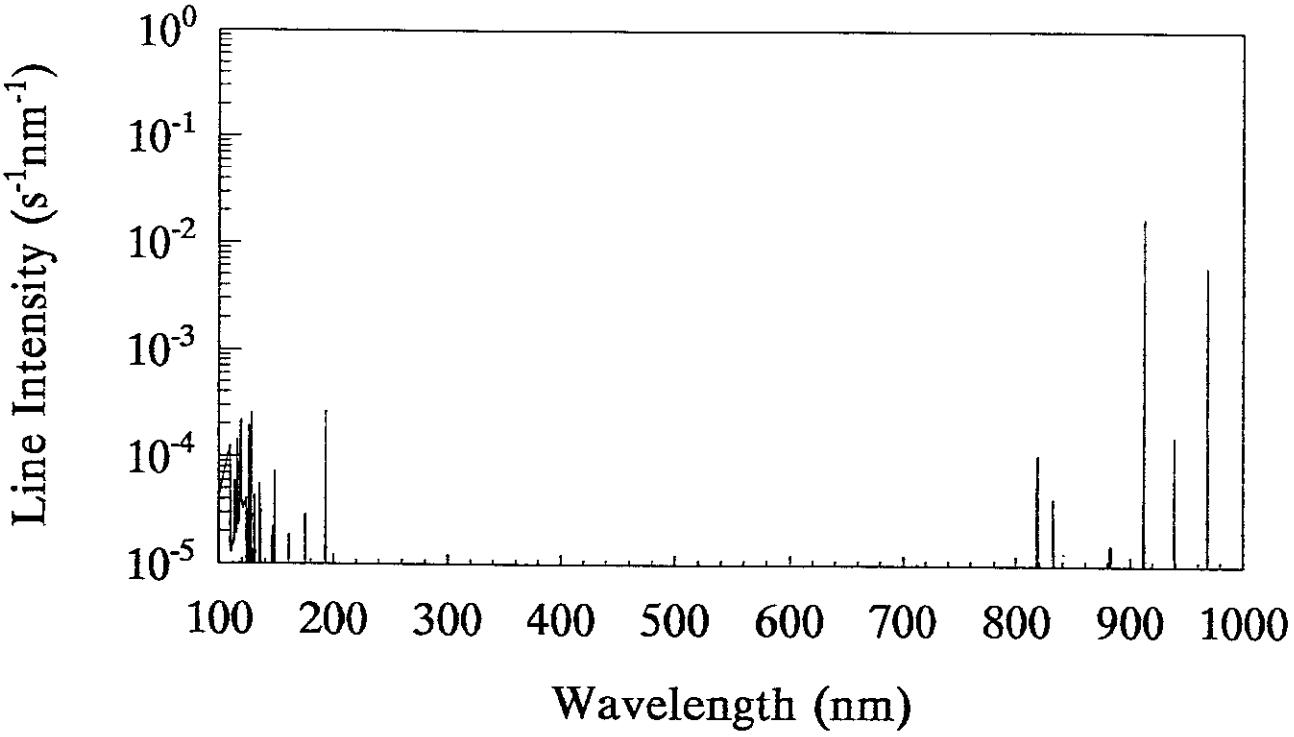

Fig.14 Spectra of neutral carbon at $T_e = 1.0eV$ and $n_e = 10^{10}cm^{-3}$ in the recombining plasma. (a). wavelength: 100-1000 nm; (b). wavelength: 100-200 nm; (c). wavelength: 550-650 nm; (d). wavelength: 900-1000 nm.

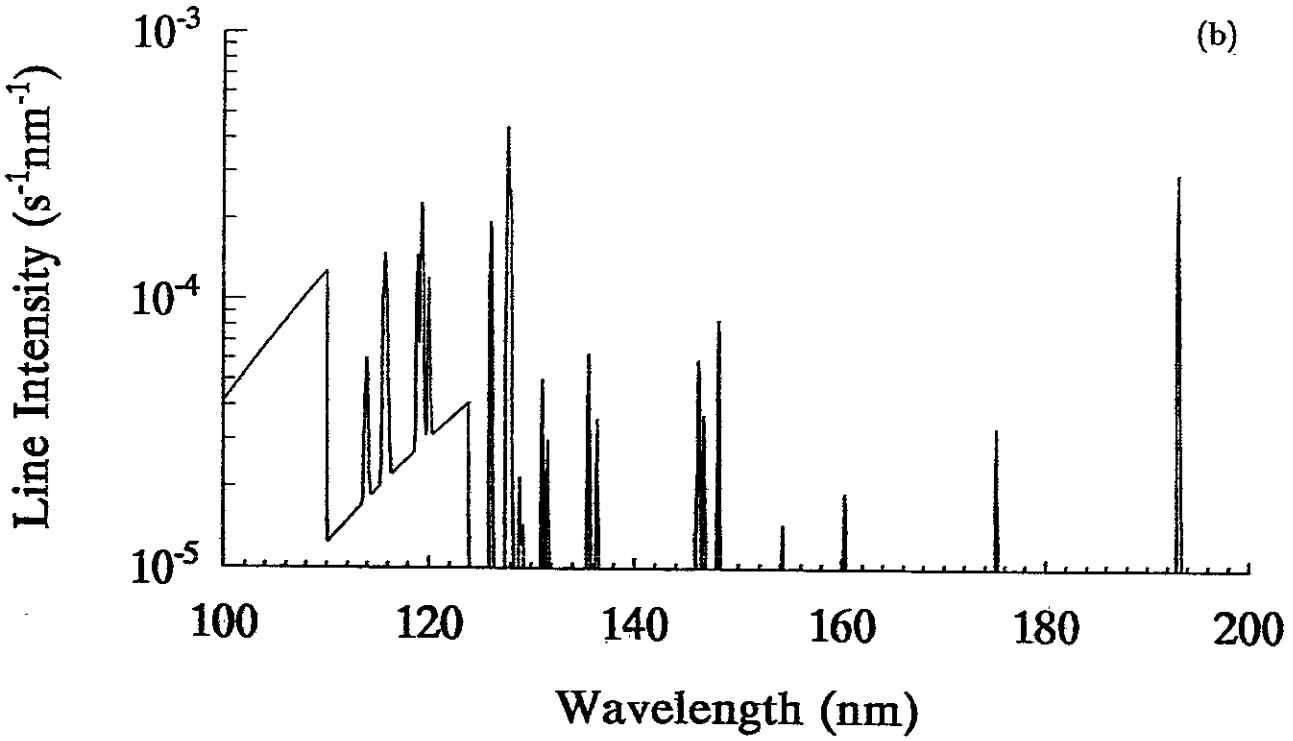

Fig.14

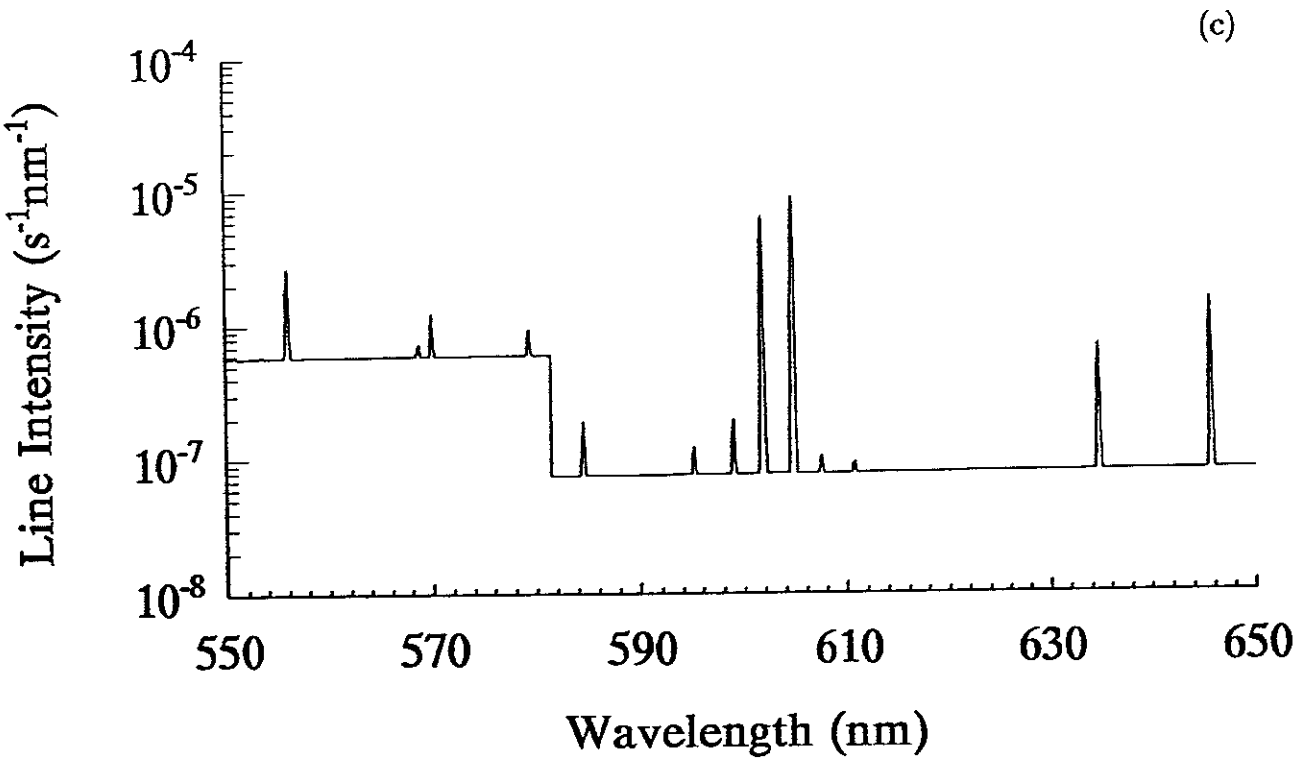
(c)
Line Intensity ($s^{-1}nm^{-1}$)
10^{-4}
10^{-5}
10^{-6}
10^{-7}
10^{-8}
550
570
590
610
630
650
Wavelength (nm)

Fig.14

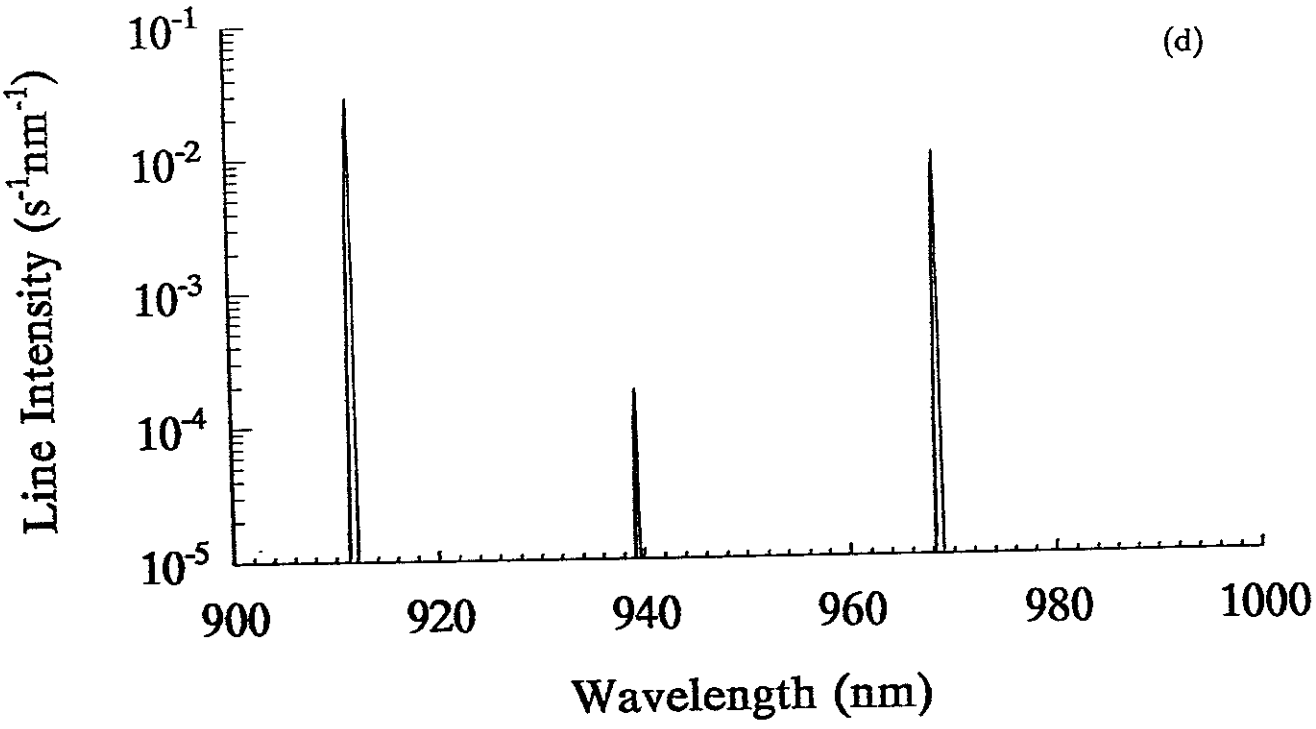
(d)
Line Intensity ($s^{-1}nm^{-1}$)
10^{-1}
10^{-2}
10^{-3}
10^{-4}
10^{-5}
900
920
940
960
980
1000
Wavelength (nm)

Fig.14

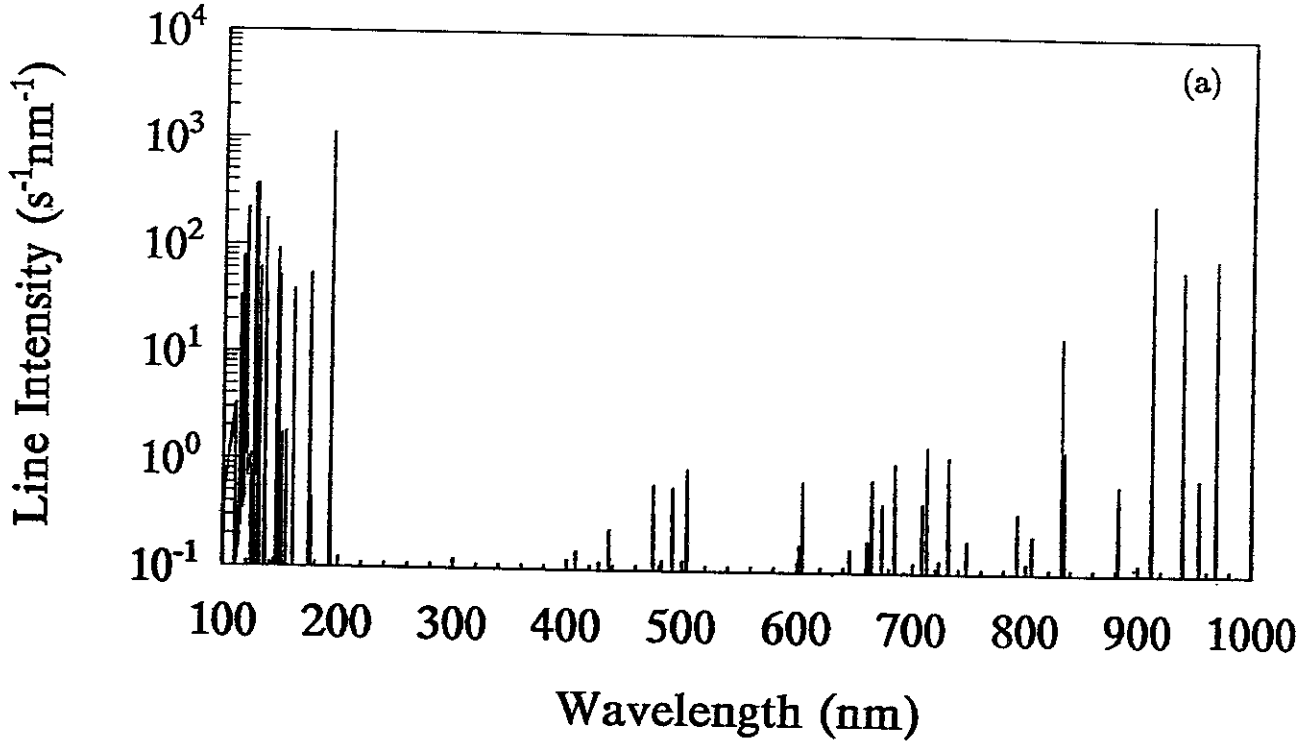

Fig.15 Spectra of neutral carbon at $T_e = 0.5eV$ and $n_e = 10^{14}cm^{-3}$ in the recombining plasma. (a). wavelength: 100-1000 nm; (b). wavelength: 100-200 nm; (c). wavelength: 550-650 nm; (d). wavelength: 900-1000 nm.

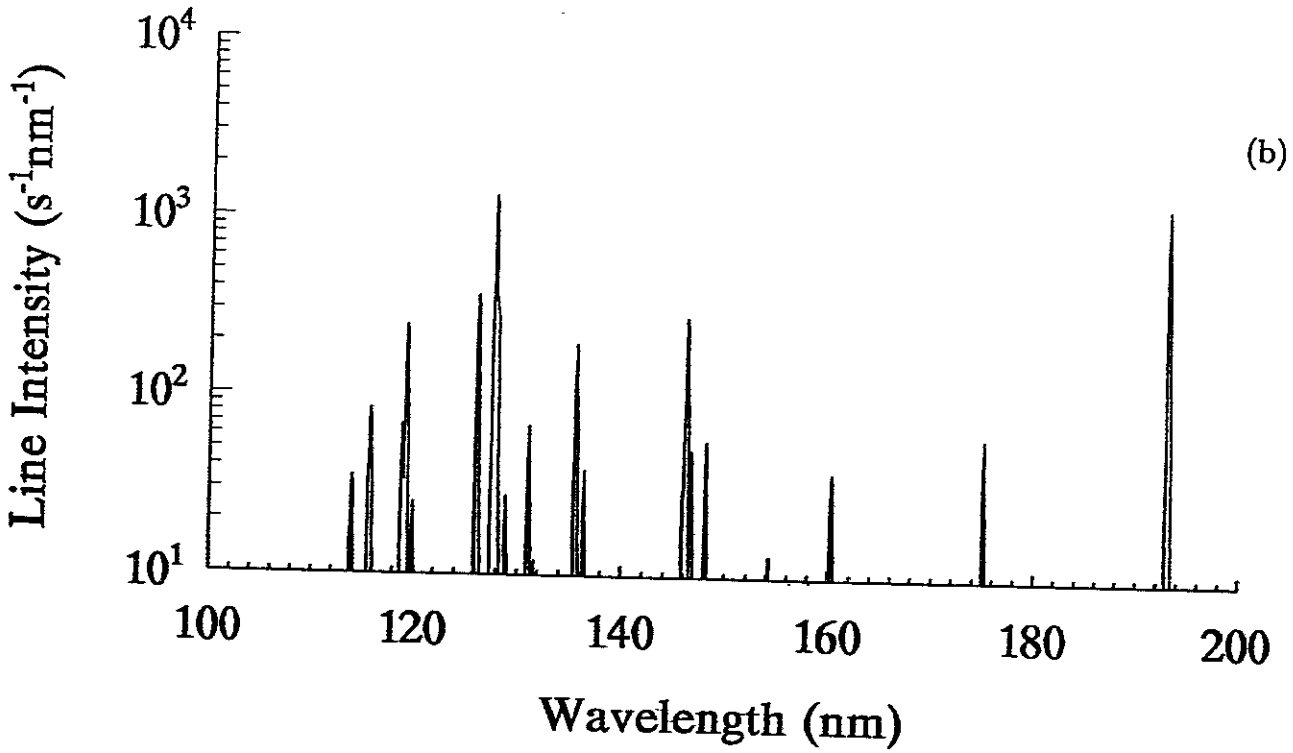

Fig.15

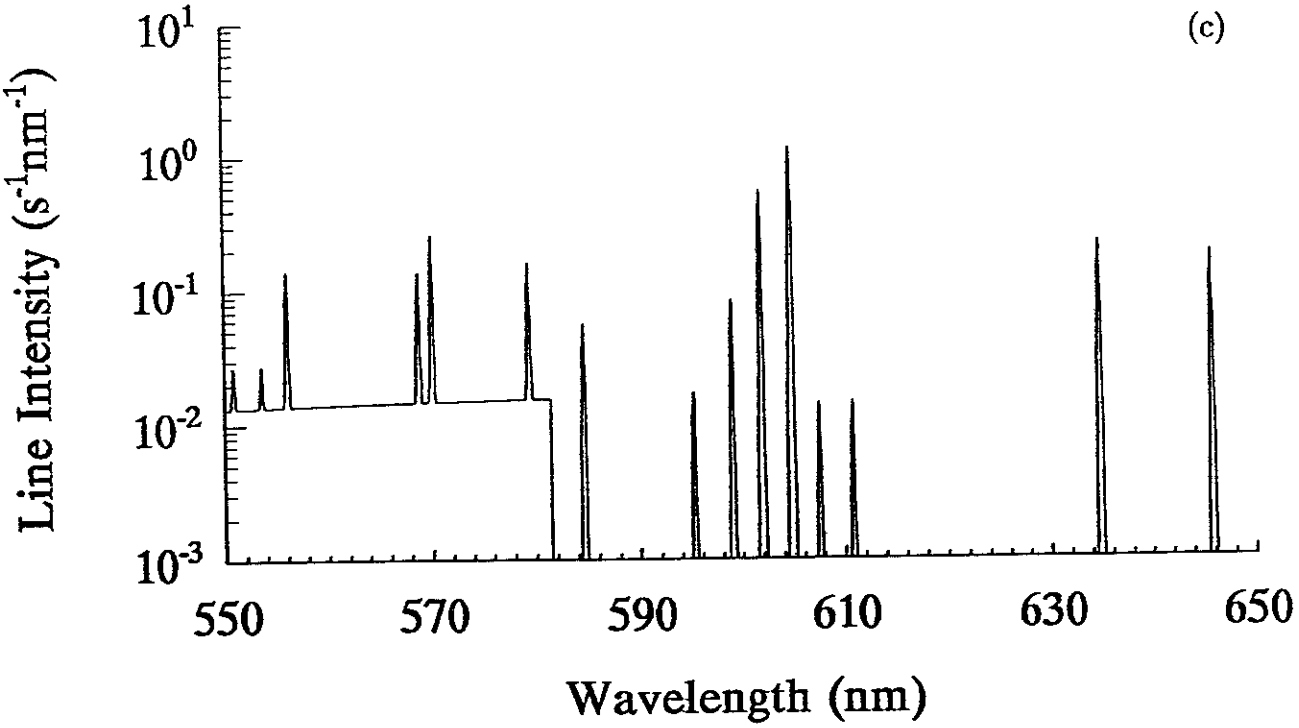
(c)
Line Intensity ($s^{-1}nm^{-1}$)
10^{1}
10^{0}
10^{-1}
10^{-2}
10^{-3}
550
570
590
610
630
650
Wavelength (nm)

Fig.15

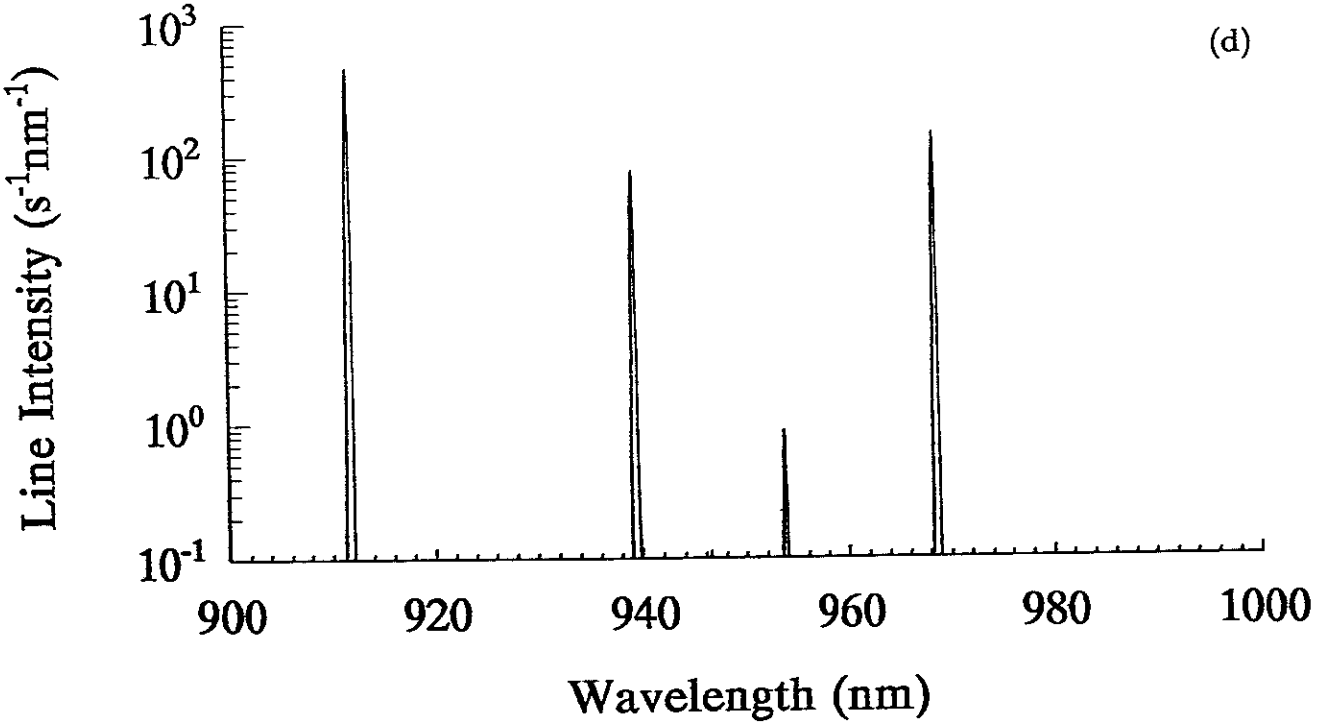
(d)
Line Intensity ($s^{-1}nm^{-1}$)
10^{3}
10^{2}
10^{1}
10^{0}
10^{-1}
900
920
940
960
980
1000
Wavelength (nm)

Fig.15

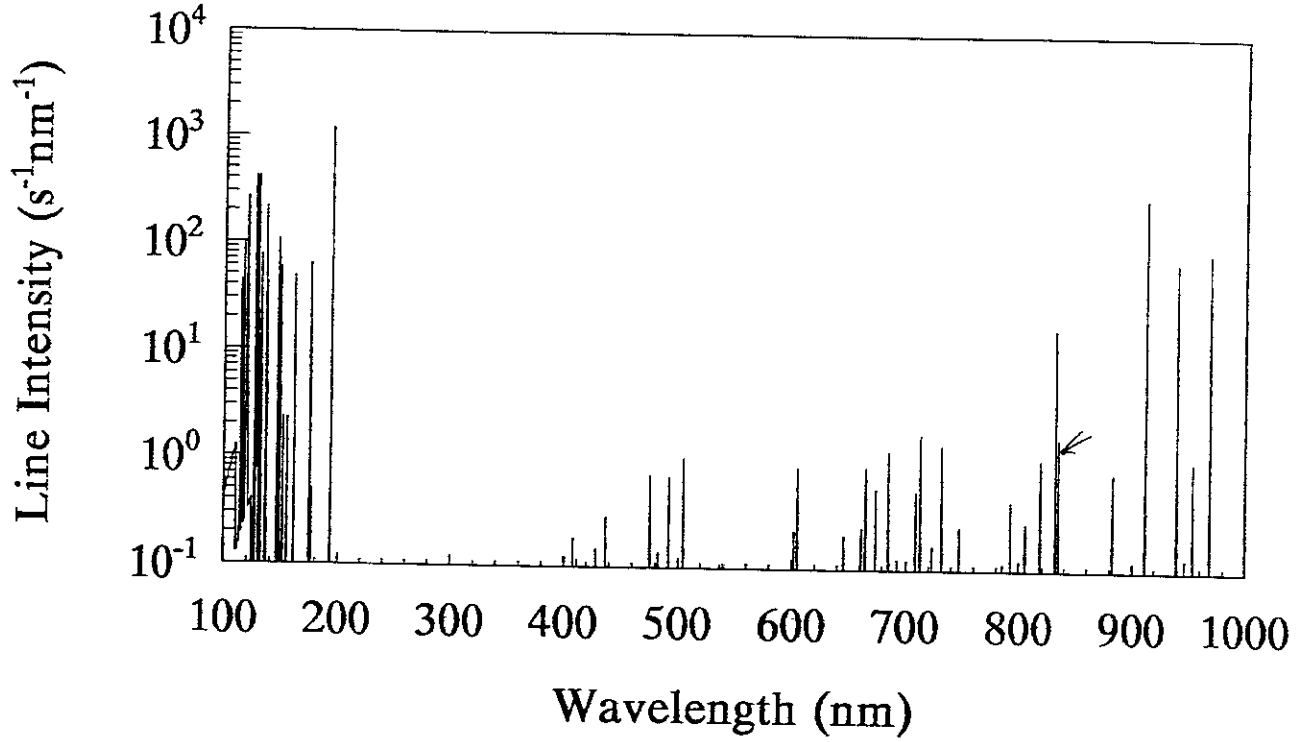

Fig.16 Spectra of neutral carbon at $T_e = 1.0eV$ and $n_e = 10^{14}cm^{-3}$ in the recombining plasma. (a). wavelength: 100-1000 nm; (b). wavelength: 100-200 nm; (c). wavelength: 550-650 nm; (d). wavelength: 900-1000 nm.

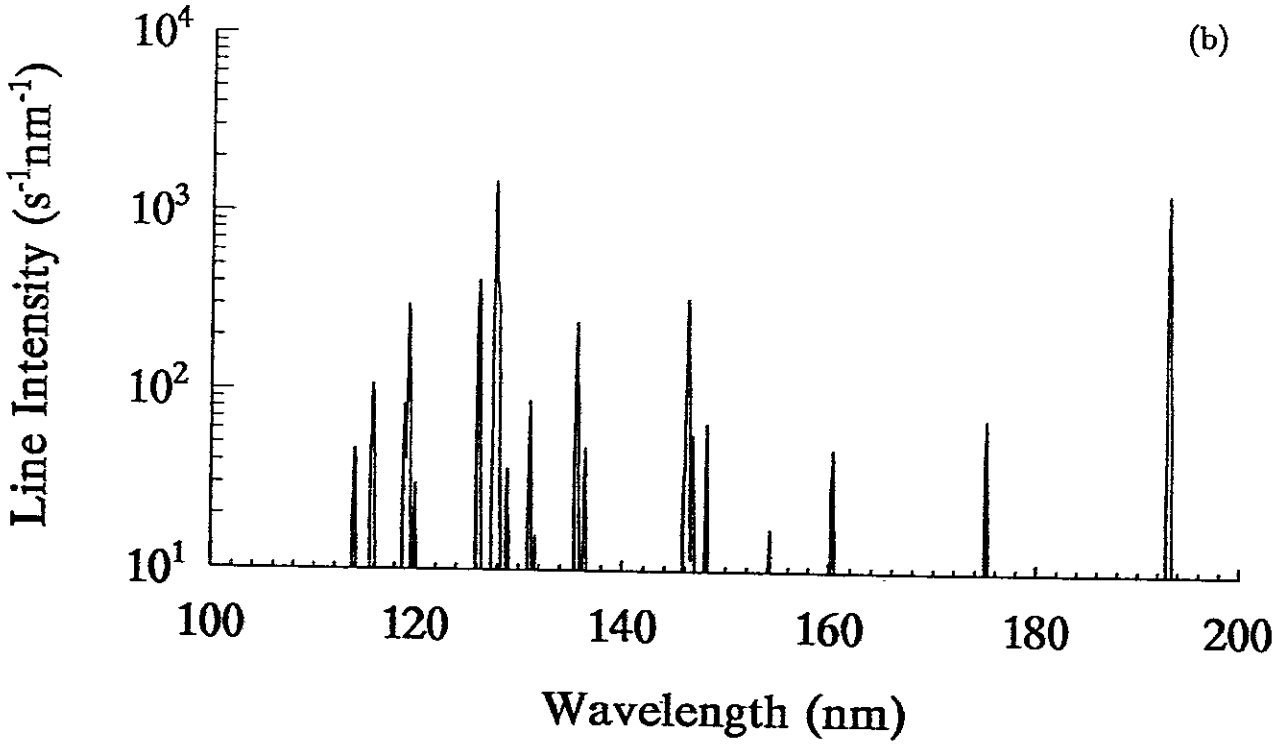

Fig.16

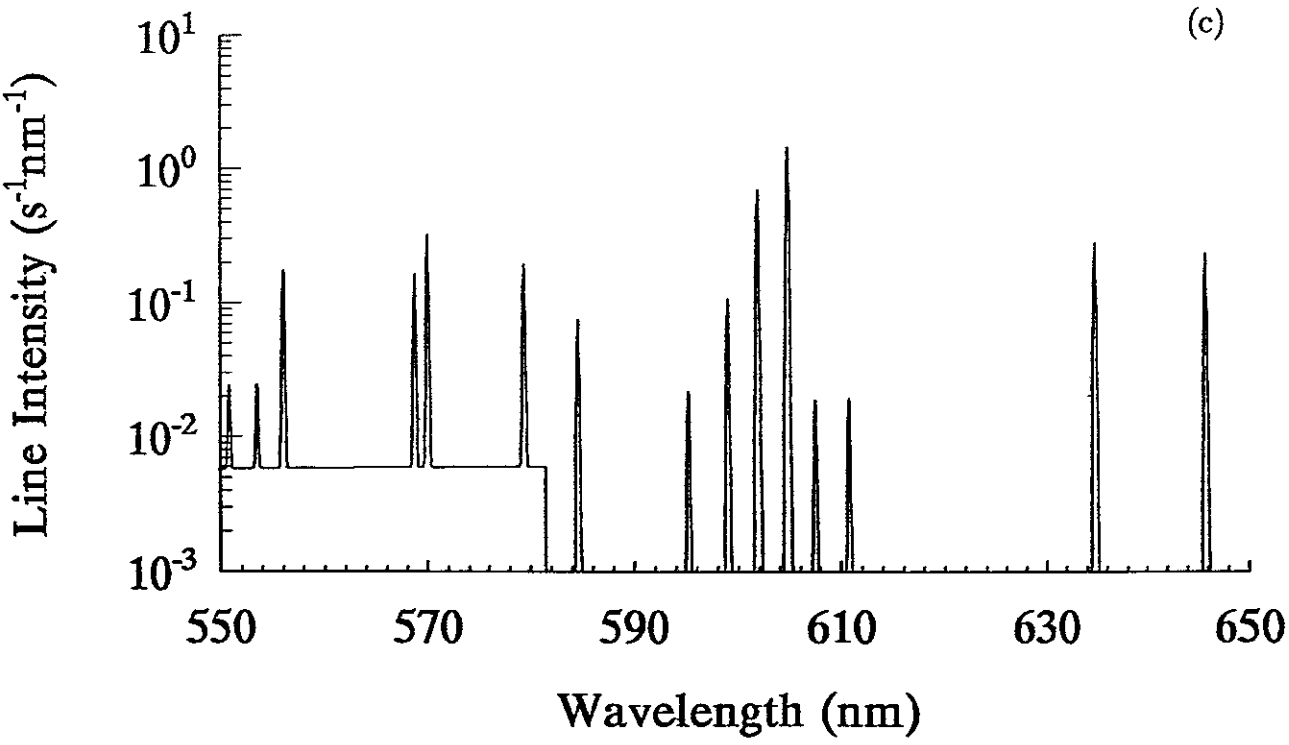
(c)
Line Intensity ($s^{-1}nm^{-1}$)
10^{1}
10^{0}
10^{-1}
10^{-2}
10^{-3}
550
570
590
610
630
650
Wavelength (nm)

Fig.16

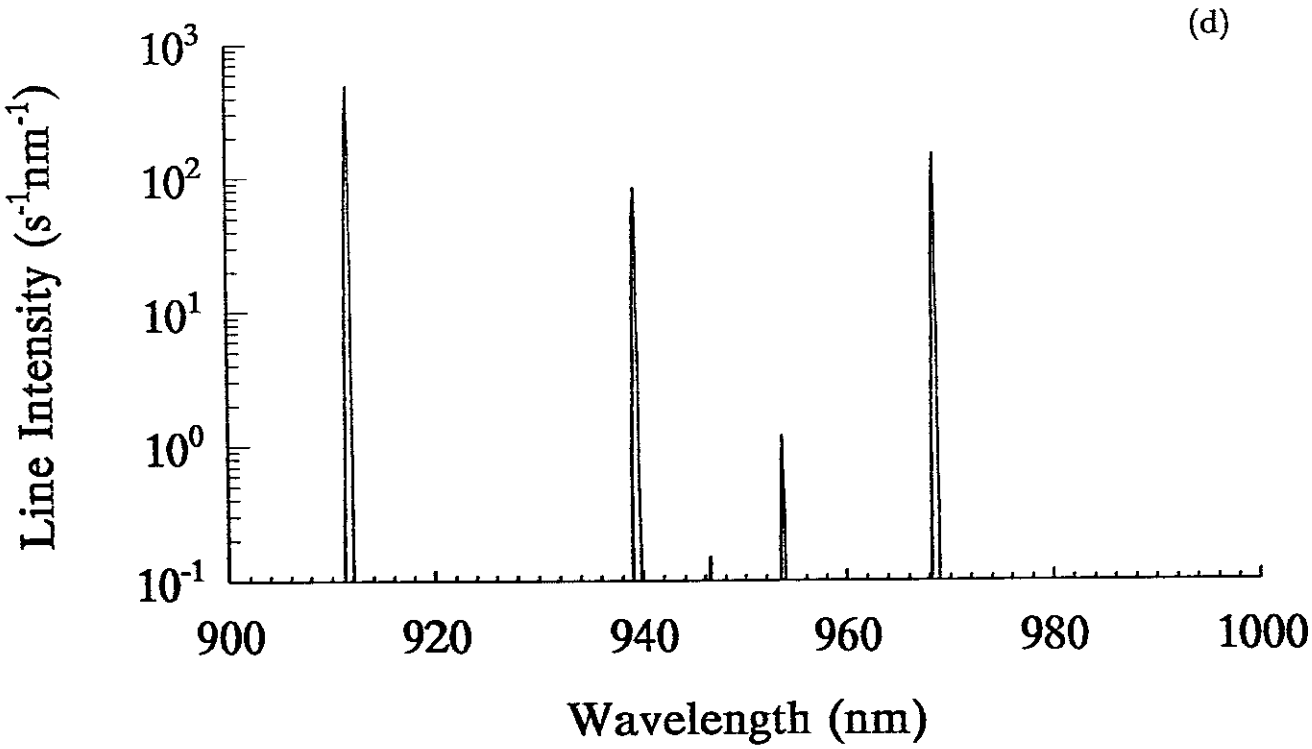
(d)
Line Intensity ($s^{-1}nm^{-1}$)
10^{3}
10^{2}
10^{1}
10^{0}
10^{-1}
900
920
940
960
980
1000
Wavelength (nm)

Fig.16

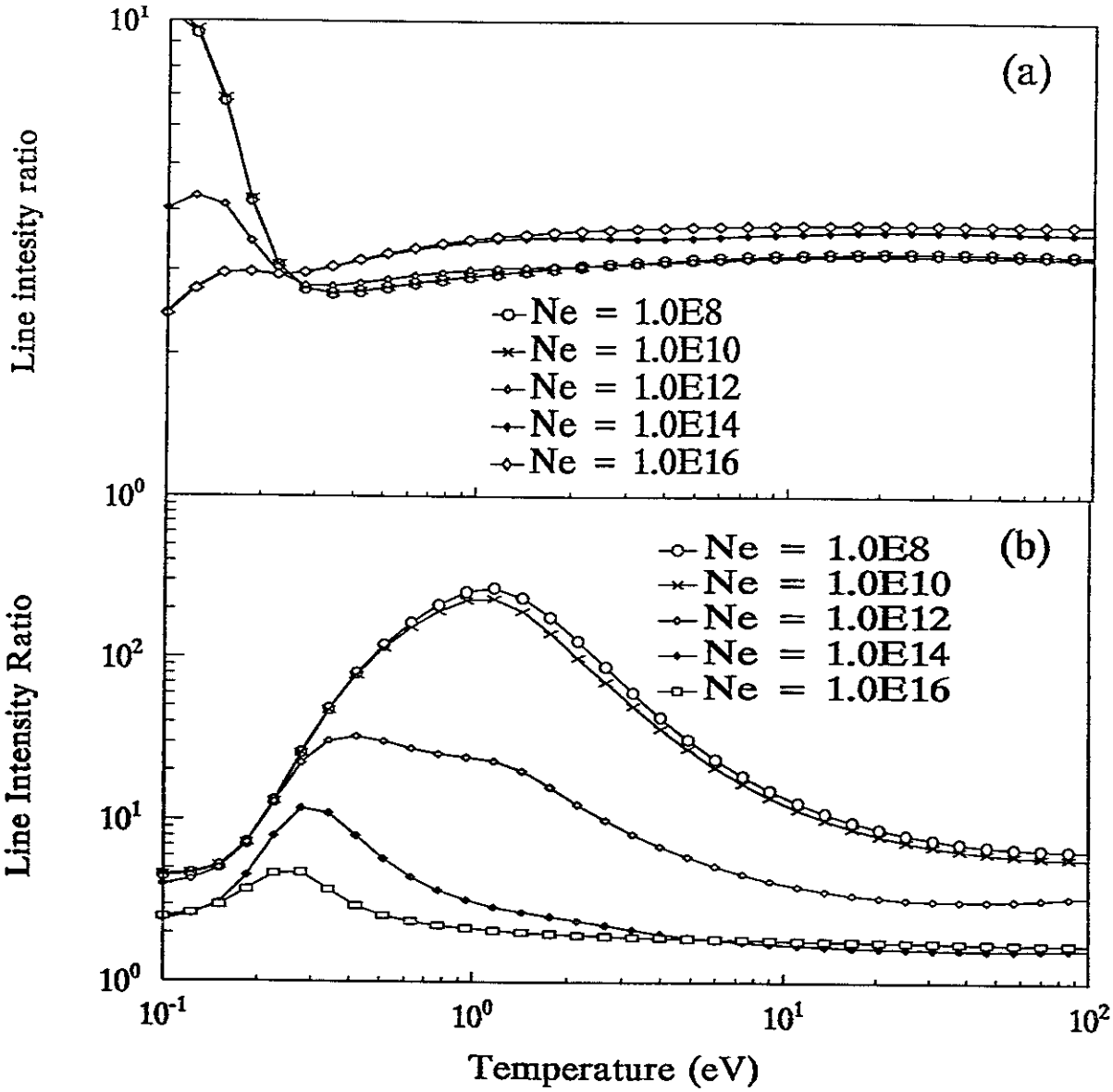

Fig.17 Line intensity ratio as a function of the electron temperature in the recombining plasma. (a). 912 nm ($2p3p(^3P) \rightarrow 2p3s(^3P)$)/968 nm ($2p3p(^3S) \rightarrow 2p3s(^3P)$); (b). 912 nm ($2p3p(^3P) \rightarrow 2p3s(^3P)$)/939 nm ($2p3p(^1D) \rightarrow 2p3s(^1P)$)

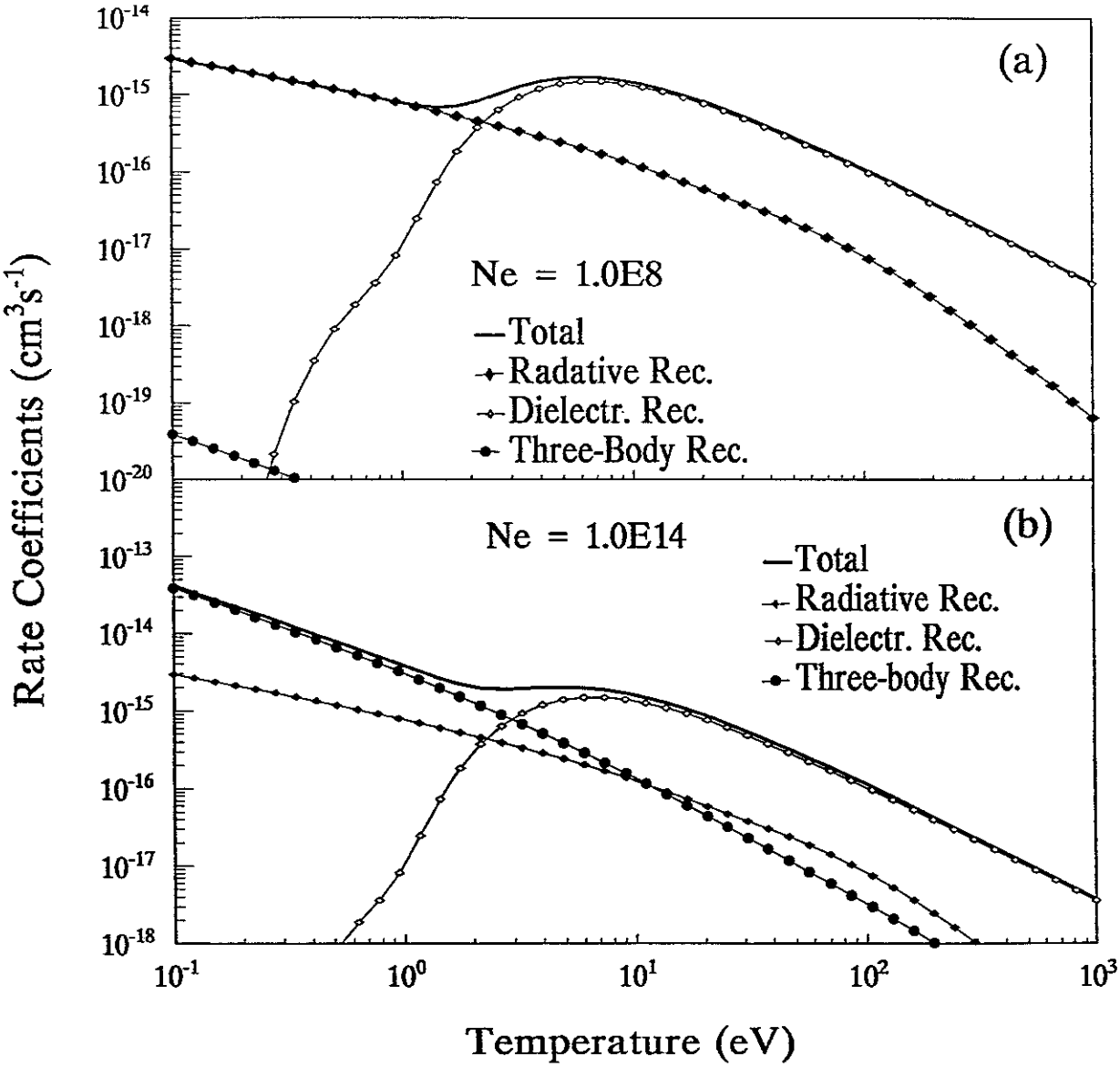

Fig.18 Recombination rate coefficients to the states $2p3p(^3P)$ as a function of the electron temperature.

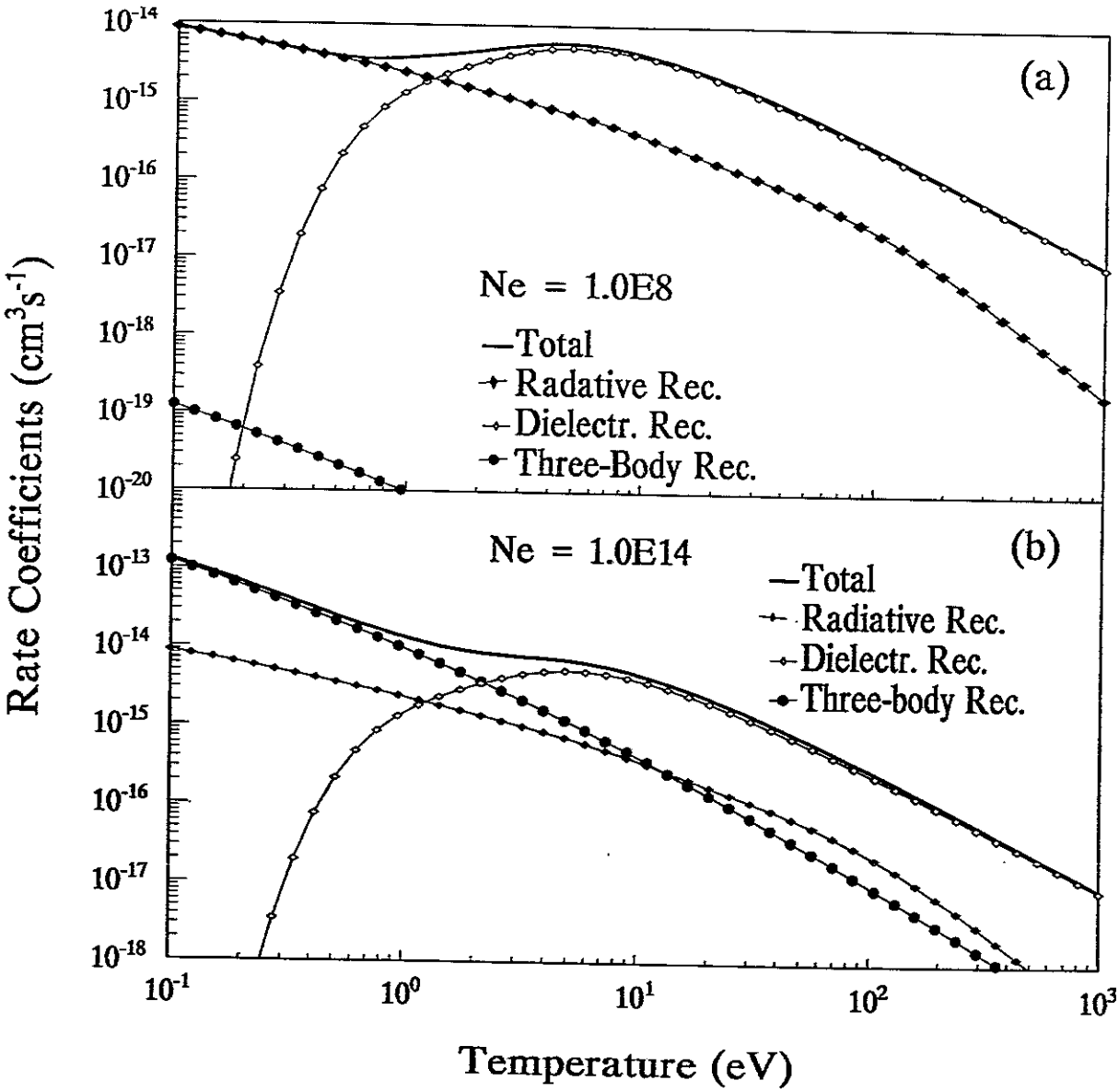

Fig.19 Recombination rate coefficients to all the states $2p3p(^3S)$ as a function of the electron temperature.

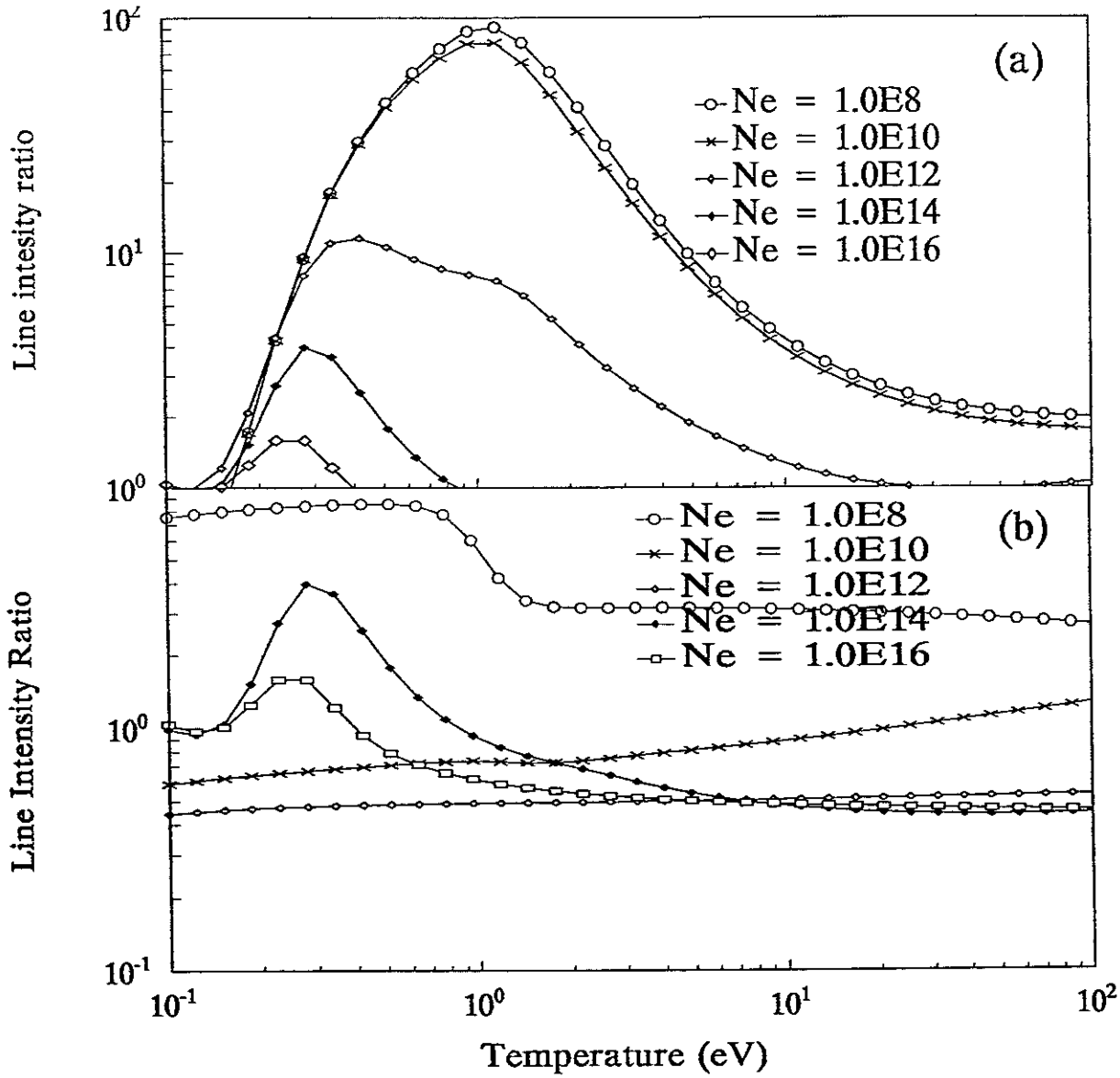

Fig.20 Line intensity ratio as a function of the electron temperature in the recombining plasma. (a). 968 nm ($2p3p(^3S) \rightarrow 2p3s(^3P)$) /939 nm ($2p3p(^1D) \rightarrow 2p3s(^1P)$) (b). 602 nm ($2p5d(^3F) \rightarrow 2p3p(^3D)$) /605 nm ($2p6s(^3P) \rightarrow 2p3p(^3D)$)

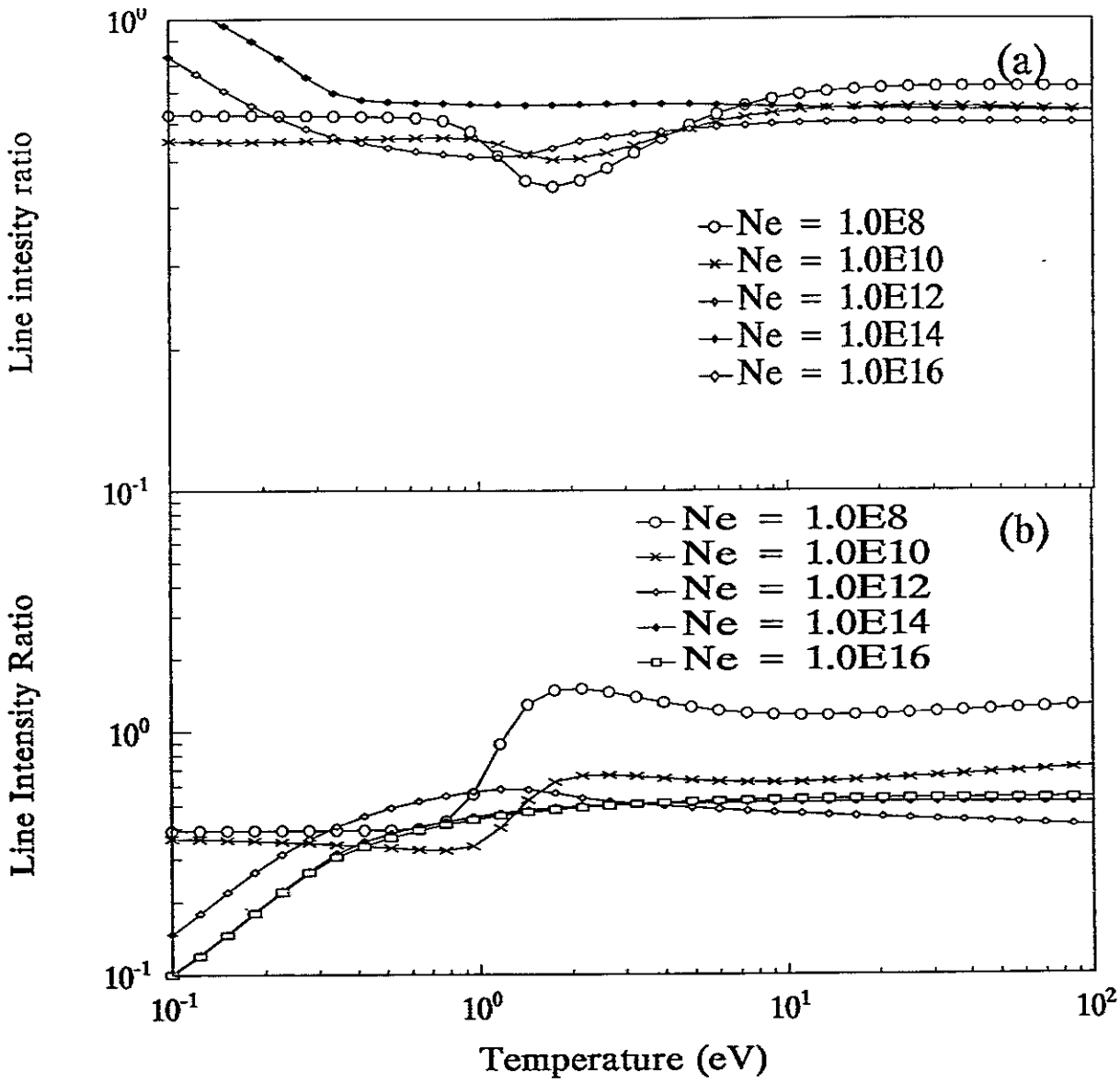

Fig.21 Line intensity ratio as a function of the electron temperature in the recombining plasma. (a). 579 nm ($2p5d(^1D) \rightarrow 2p3p(^1P)$) /635 nm ($2p5d(^3P) \rightarrow 2p3p(^3S)$) (b). 585 nm ($2p6d(^3P) \rightarrow 2p3p(^3S)$) /579 nm ($2p5d(^1D) \rightarrow 2p3p(^1P)$)

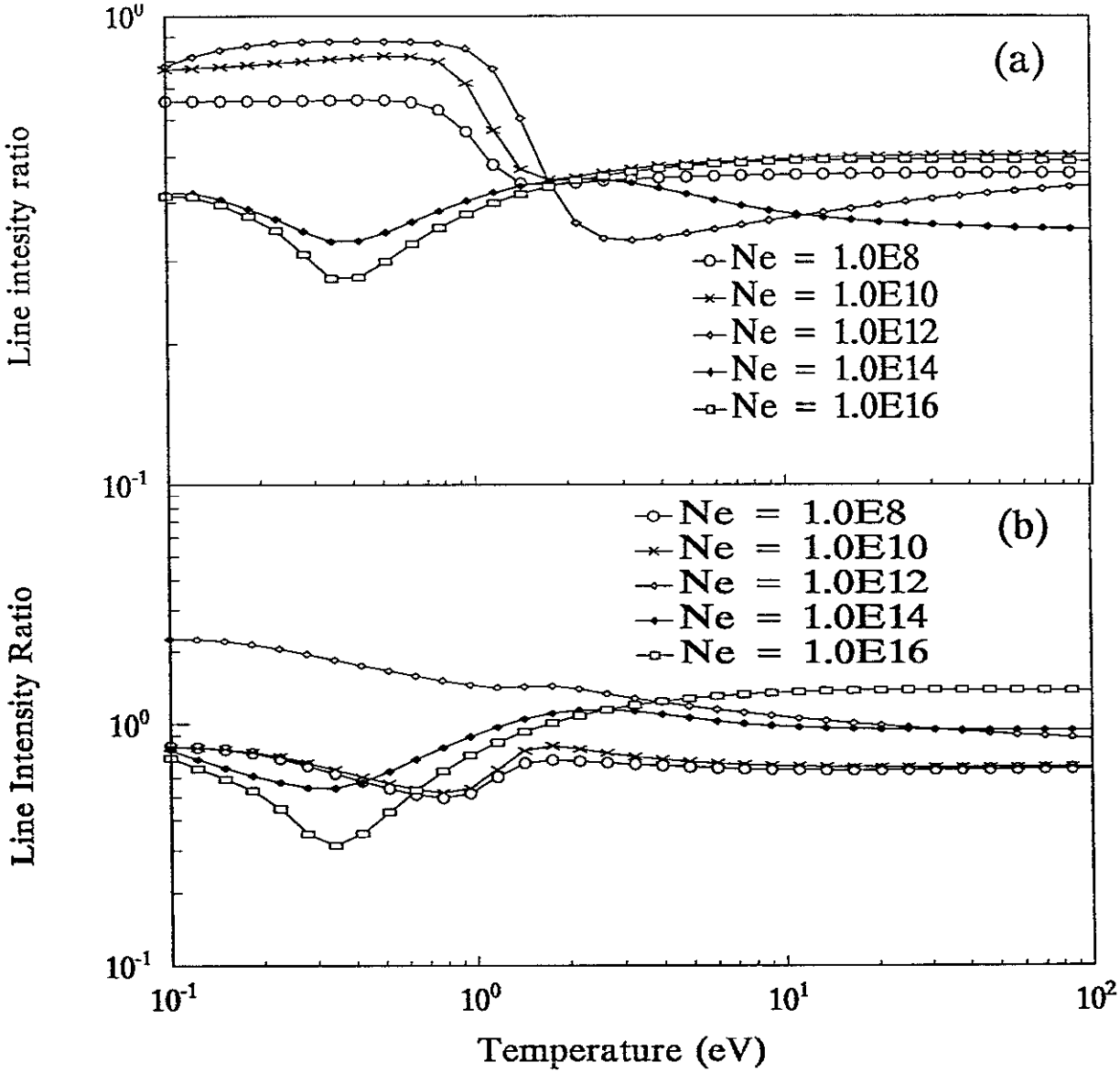

Fig.22 Line intensity ratio as a function of the electron temperature in the recombining plasma. (a). 156 nm ($2p5d(^1P) \rightarrow 2p^2(^1S)$) /160 nm ($2p4d(^1P) \rightarrow 2p^2(^1S)$) (b). 160 nm ($2p4d(^1P) \rightarrow 2p^2(^1S)$) /175 nm ($2p3d(^1P) \rightarrow 2p^2(^1S)$)

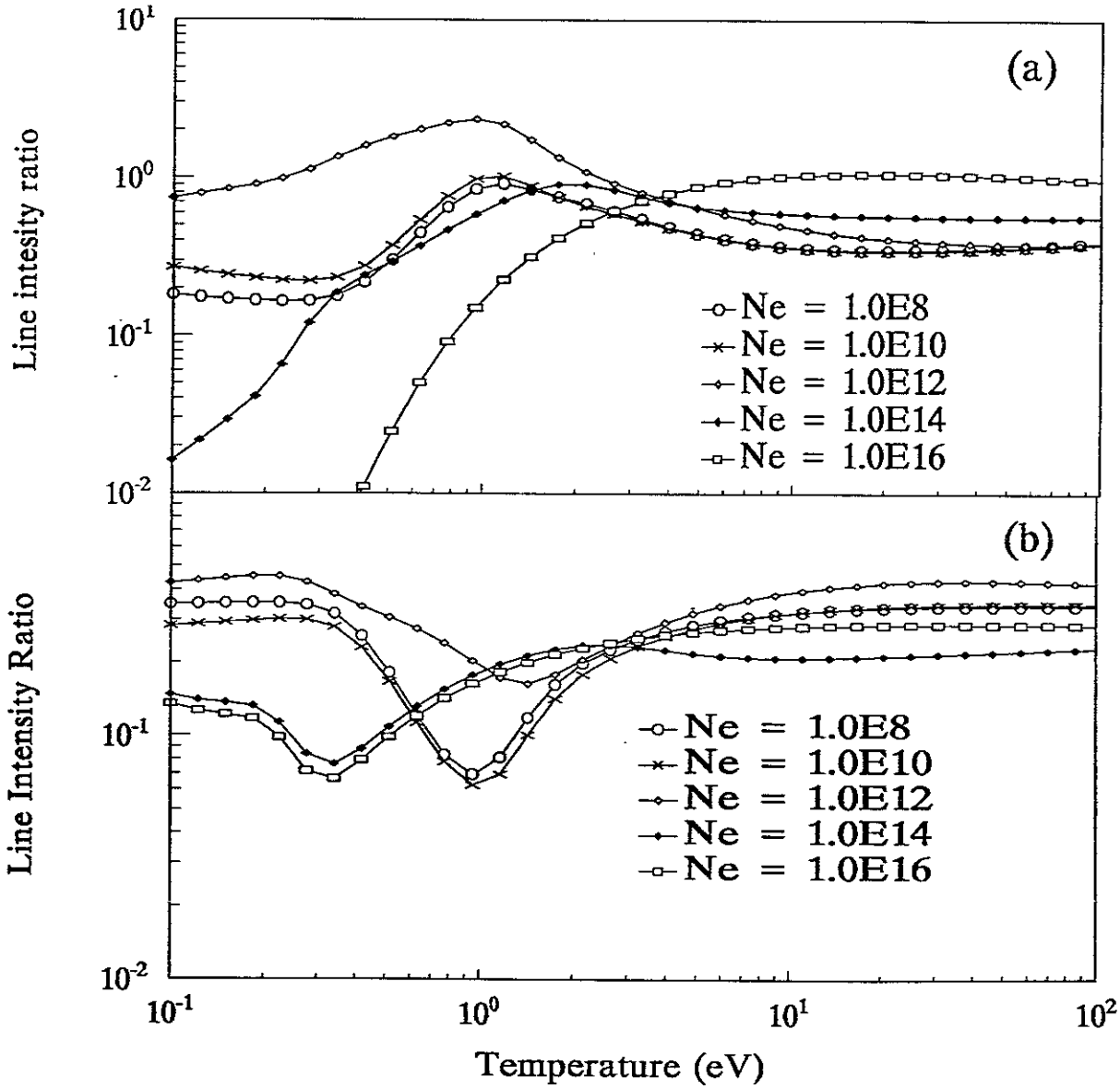

Fig.23 Line intensity ratio as a function of the electron temperature in the recombining plasma. (a). 126 nm ($2p3d(^3P) \rightarrow 2p^2(^3P)$) /193 nm ($2p3s(^1P) \rightarrow 2p^2(^1D)$) (b). 160 nm ($2p4d(^1P) \rightarrow 2p^2(^1S)$) /126 nm ($2p3d(^3P) \rightarrow 2p^2(^3P)$)

Publication List of NIFS-DATA Series

NIFS-DATA-1 Y. Yamamura, T. Takiguchi and H. Tawara,
Data Compilation of Angular Distributions of Sputtered Atoms; Jan 1990

NIFS-DATA-2 T. Kato, J. Lang and K. E. Berrington,
Intensity Ratios of Emission Lines from OV Ions for Temperature and Density Diagnostics ; Mar. 1990 [At Data and Nucl Data Tables 44(1990)133]

NIFS-DATA-3 T. Kaneko,
Partial Electronic Straggling Cross Sections of Atoms for Protons; Mar. 1990

NIFS-DATA-4 T Fujimoto, K. Sawada and K. Takahata,
Cross Section for Production of Excited Hydrogen Atoms Following Dissociative Excitation of Molecular Hydrogen by Electron Impact ; Mar. 1990

NIFS-DATA-5 H. Tawara,
Some Electron Detachment Data for H^- Ions in Collisions with Electrons, Ions, Atoms and Molecules – an Alternative Approach to High Energy Neutral Beam Production for Plasma Heating– ;Apr. 1990

NIFS-DATA-6 H Tawara, Y. Itikawa, H. Nishimura, H Tanaka and Y Nakamura,
Collision Data Involving Hydro-Carbon Molecules ; July 1990 [Supplement to Nucl. Fusion 2(1992)25; Atomic and Molecular Processes in Magnetic Fusion Edge Plasmas (Plenum, 1995) p461]

NIFS-DATA-7 H.Tawara,
Bibliography on Electron Transfer Processes in Ion-Ion/Atom/Molecule Collisions –Updated 1990–, Aug. 1990

NIFS-DATA-8 U.I.Safronova, T.Kato, K.Masai, L.A.Vainshtein and A S Shlyapzeva,
Excitation Collision Strengths, Cross Sections and Rate Coefficients for OV, SiXI, FeXXIII, MoXXXIX by Electron Impact ($1s^22s^2$ - $1s^22s2p$-$1s^22p^2$ Transitions) Dec.1990

NIFS-DATA-9 T.Kaneko,
Partial and Total Electronic Stopping Cross Sections of Atoms and Solids for Protons; Dec. 1990

NIFS-DATA-10 K Shima, N.Kuno, M.Yamanouchi and H.Tawara,
Equilibrium Charge Fraction of Ions of Z=4-92 (0.02-6 MeV/u) and Z=4-20 (Up to 40 MeV/u) Emerging from a Carbon Foil; Jan.1991 [AT.Data and Nucl. Data Tables 51(1992)173]

NIFS-DATA-11 T. Kaneko, T. Nishihara, T Taguchi, K. Nakagawa, M. Murakami, M. Hosono, S. Matsushita, K. Hayase, M.Moriya, Y.Matsukuma, K.Miura and Hiro Tawara,
Partial and Total Electronic StoppingCross Sections of Atoms for a Singly Charged Helium Ion: Part 1;
Mar. 1991

NIFS-DATA-12 Hiro Tawara,
Total and Partial Cross Sections of Electron Transfer Processes for Be^{q+} and B^{q+} Ions in Collisions with H, H_2 and He Gas Targets -Status in 1991-; June 1991

NIFS-DATA-13 T. Kaneko, M. Nishikori, N Yamato, T. Fukushima, T. Fujikawa, S Fujita, K Miki, Y. Mitsunobu, K. Yasuhara, H. Yoshida and Hiro Tawara,
Partial and Total Electronic Stopping Cross Sections of Atoms for a Singly Charged Helium Ion : Part II; Aug. 1991

NIFS-DATA-14 T. Kato, K. Masai and M. Arnaud,
Comparison of Ionization Rate Coefficients of Ions from Hydrogen through Nickel ; Sep 1991

NIFS-DATA-15 T. Kato, Y. Itikawa and K. Sakimoto,
Compilation of Excitation Cross Sections for He Atoms by Electron Impact; Mar. 1992

NIFS-DATA-16 T. Fujimoto, F. Koike, K. Sakimoto, R. Okasaka, K. Kawasaki, K. Takiyama, T. Oda and T. Kato,
Atomic Processes Relevant to Polarization Plasma Spectroscopy ; Apr. 1992

NIFS-DATA-17 H. Tawara,
Electron Stripping Cross Sections for Light Impurity Ions in Colliding with Atomic Hydrogens Relevant to Fusion Research; Apr. 1992

NIFS-DATA-18 T. Kato,
Electron Impact Excitation Cross Sections and Effective Collision Strengths of N Atom and N-Like Ions -A Review of Available Data and Recommendations- ; Sep. 1992 [Atomic Data and Nuclear Data Tables, 57, 181-214 (1994)]

NIFS-DATA-19 Hiro Tawara,
Atomic and Molecular Data for H_2O, CO & CO_2 Relevant to Edge Plasma Impurities , Oct. 1992

NIFS-DATA-20 Hiro. Tawara,
Bibliography on Electron Transfer Processes in Ion-Ion/Atom/Molecule Collisions - Updated 1993-;
Apr. 1993

NIFS-DATA-21 J. Dubau and T. Kato,
Dielectronic Recombination Rate Coefficients to the Excited States of C I from C II; Aug. 1994

NIFS-DATA-22 T. Kawamura, T. Ono, Y. Yamamura,
Simulation Calculations of Physical Sputtering and Reflection Coefficient of Plasma-Irradiated Carbon Surface;Aug. 1994 [J. Nucl. Mater., 220 (1995) 1010]

NIFS-DATA-23 Y. Yamamura and H. Tawara,
Energy Dependence of Ion-Induced Sputtering Yields from Monoatomic Solids at Normal Incidence; Mar. 1995 [At. Data and Nucl. Data Tables, 62 (1996) 149]

NIFS-DATA-24 T. Kato, U. Safronova, A. Shlyaptseva, M. Comille, J. Dubau,
Comparison of the Satellite Lines of H-like and He-like Spectra; Apr. 1995 [Atomic Data and Nuclear Data Tables, 67., 225 (1997)]

NIFS-DATA-25 H. Tawara,
Roles of Atomic and Molecular Processes in Fusion Plasma Researches - from the cradle (plasma production) to the grave (after-burning) -; May 1995

NIFS-DATA-26 N. Toshima and H. Tawara
Excitation, Ionization, and Electron Capture Cross Sections of Atomic Hydrogen in Collisions with Multiply Charged Ions; July 1995

NIFS-DATA-27 V.P. Shevelko, H. Tawara and E.Salzborn,
Multiple-Ionization Cross Sections of Atoms and Positive Ions by Electron Impact; July 1995 [Suppl. Nucl. Fusion, 6 (1996) 101]

NIFS-DATA-28 V.P. Shevelko and H. Tawara,
Cross Sections for Electron-Impact Induced Transitions Between Excited States in He:

n, n'=2,3 and 4; Aug. 1995 [Suppl. Nucl. Fusion, 6 (1996) 27]

NIFS-DATA-29 U.I. Safronova, M.S. Safronova and T Kato,
Cross Sections and Rate Coefficients for Excitation of $\Delta n = 1$ Transitions in Li-like Ions with $6<Z<42$; Sep. 1995 [Physica Scripta, 54, 68-84 (1996)]

NIFS-DATA-30 T. Nishikawa, T. Kawachi, K. Nishihara and T. Fujimoto,
Recommended Atomic Data for Collisional-Radiative Model of Li-like Ions and Gain Calculation for Li-like Al Ions in the Recombining Plasma; Sep. 1995

NIFS-DATA-31 Y. Yamamura, K. Sakaoka and H Tawara,
Computer Simulation and Data Compilation of Sputtering Yield by Hydrogen Isotopes ($^1H^+$, $^2D^+$, $^3T^+$) and Helium ($^4He^+$) Ion Impact from Monatomic Solids at Normal Incidence; Oct. 1995

NIFS-DATA-32 T. Kato, U. Safronova and M. Ohira,
Dielectronic Recombination Rate Coefficients to the Excited States of CII from CIII; Feb. 1996 [Physica Scripta, 53, 461-472 (1996), Physica Scripta, 55, 185-199 (1997)]

NIFS-DATA-33 K.J. Snowdon and H. Tawara,
Low Energy Molecule-Surface Interaction Processes of Relevance to Next-Generation Fusion Devices;
Mar. 1996 [Comm. At. Mol. Opt. Phys. 34 (1998) 21]

NIFS-DATA-34 T. Ono, T. Kawamura, K. Ishii and Y. Yamamura,
Sputtering Yield Formula for B_4C Irradiated with Monoenergetic Ions at Normal Incidence; Apr. 1996 [J. Nucl. Mater., 232 (1996) 52]

NIFS-DATA-35 I. Murakami, T. Kato and J. Dubau,
UV and X-Ray Spectral Lines of Be-Like Fe Ion for Plasma Diagnostics; Apr. 1996 [Physica Scripta, 54, 463-470 (1996)]

NIFS-DATA-36 K. Moribayashi and T. Kato,
Dielectronic Recombination of Be-like Fe Ion; Apr. 1996 [Physca Scripta Vol.55, 286-297 (1997)]

NIFS-DATA-37 U. Safronova, T Kato and M Ohira,
Dielectronic Recombination Rate Coefficients to the Excited States of CIII from CIV; July 1996 [J. Quant. Spectrosc. Radiat. Transfer, 58, 193 - 215, (1997)]

NIFS-DATA-38 T. Fujimoto, H. Sahara, G. Csanak and S Grabbe,
Atomic States and Collisional Relaxation in Plasma Polarization Spectroscopy: Axially Symmetric Case; Oct. 1996

NIFS-DATA-39 H Tawara (Ed)
Present Status on Atomic and Molecular Data Relevant to Fusion Plasma Diagnostics and Modeling;
Jan. 1997

NIFS-DATA-40 Inga Yu. Tolstikhina,
LS-Averaged 1/Z Method as a Tool of Studying the Interactions of Highly Charged Ions with a Metal Surface; Jan. 1997

NIFS-DATA-41 K Moribayashi and T Kato,
Atomic Nuclear Charge Scaling for Dielectronic Recombination to Be- like Ions; Apr. 1997

NIFS-DATA-42 H Tawara,
Bibliography on Electron Transfer Processes in Ion-ion / Atom / Molecule Collisions -

Updated 1997 -; May 1997

NIFS-DATA-43 M. Goto and T. Fujimoto,
Collisional-radiative Model for Neutral Helium in Plasma: Excitation Cross Section and Singlet-triplet Wavefunction Mixing; Oct. 1997

NIFS-DATA-44 J. Dubau, T. Kato and U.I. Safronova,
Dielectronic Recombination Rate Coefficients to the Excited States of Cl From ClI; Jan. 1998

NIFS-DATA-45 Y. Yamamura, W. Takeuchi and T. Kawamura,
The Screening Length of Interatomic Potential in Atomic Collisions; Mar. 1998

NIFS-DATA-46 T Kenmotsu, T Kawamura, T. Ono and Y Yamamura,
Dynamical Simulation for Sputtering of B4C; Mar. 1998

NIFS-DATA-47 I. Murakami, K. Moribayashi and T. Kato,
Effect of Recombination Processes on FeXXIII Line Intensities; May 1998

NIFS-DATA-48 Zhijie Li, T. Kenmotsu, T. Kawamura, T. Ono and Y. Yamamura,
Sputtering Yield Calculations Using an Interatomic Potential with the Shell Effect and a New Local Model; Oct. 1998

NIFS-DATA-49 S. Sasaki, M. Goto, T. Kato and S. Takamura,
Line Intensity Ratios of Helium Atom in an Ionizing Plasma; Oct. 1998

NIFS-DATA-50 I. Murakami, T Kato and U. Safronova,
Spectral Line Intensities of NeVII for Non-equilibrium Ionization Plasma Including Dielectronic Recombination Processses; Jan. 1999

NIFS-DATA-51 Hiro Tawara and Masa Kato,
Electron Impact Ionization Data for Atoms and Ions -up-dated in 1998-; Feb. 1999

NIFS-DATA-52 J.G. Wang, T. Kato and I. Murakami,
Validity of n^{-3} Scaling Law in Dielectronic Recombination Processes; Apr. 1999

NIFS-DATA-53 J.G. Wang, T. Kato and I. Murakami,
Dielectronic Recombination Rate Coefficients to Excited States of He from He^{+}; Apr. 1999

NIFS-DATA-54 T. Kato and E. Asano,
Comparison of Recombination Rate Coefficients Given by Empirical Formulas for Ions from Hydrogen through Nickel; June 1999

NIFS-DATA-55 H.P. Summers, H. Anderson, T. Kato and S. Murakami,
Hydrogen Beam Stopping and Beam Emission Data for LHD; Nov. 1999

NIFS-DATA-56 S. Born, N. Matsunami and H. Tawara,
A Simple Theoretical Approach to Determine Relative Ion Yield (RIY) in Glow Discharge Mass Spectrometry (GDMS); Jan. 2000

NIFS-DATA-57 T. Ono, T. Kawamura, T. Kenmotsu, Y. Yamamura,
Simulation Study on Retention and Reflection from Tungsten Carbide under High Fluence of Helium Ions; Aug. 2000

NIFS-DATA-58 J.G. Wang, M. Kato and T. Kato,
Spectra of Neutral Carbon for Plasma Diagnostics; Oct. 2000